American Petroleum Institute

Models for Design of Free-Product Recovery Systems for Petroleum Hydrocarbon Liquids

Regulatory Analysis and Scientific Affairs Department

PUBLICATION NUMBER 4729
AUGUST 2003

Free-Product Recovery System Analysis

$t_{recovery}$ [yr] =	3
R_c [ft] =	40
μ_o [cp] =	2
K_w [ft/d] =	15
r_{well} [ft] =	0.5

Water Enhanced	
Q_w [gpm] =	5
b_{well} [ft] =	15
$R_{Influence}$ [ft] =	200
s_{well} [ft] =	4.08

Vacuum Enhanced	
(-) p_w [atm]	0
L_{well} [ft] =	5
k_{ra} =	0.9
Q_{air} [scfm] =	0.0
h_{well} [ft H_2O] =	0.00

Skimmer Well

If $Q_w = 0$ and $p_w = 0$ then a skimmer well is assumed

Average drawdown (buildup) within radius of capture

s_c [ft] = 1.44

Press Ctrl-Shift+S to calculate sheet

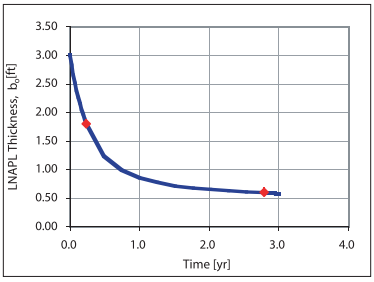

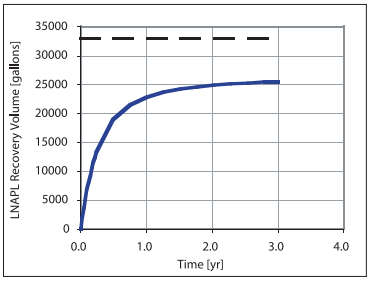

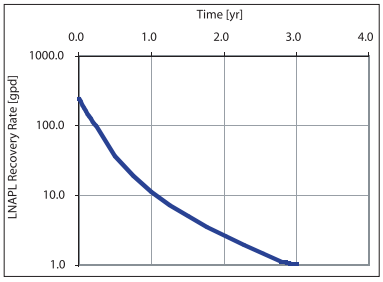

Models for Design of Free-Product Recovery Systems for Petroleum Hydrocarbon Liquids

Regulatory Analysis and Scientific Affairs Department

API PUBLICATION 4729

PREPARED UNDER CONTRACT BY:

Randall J. Charbeneau
Environmental and Water Resources Engineering Program
College of Engineering
The University of Texas at Austin

August 2003

American Petroleum Institute

Helping You Get The Job Done Right.SM

FORWARD

API publications may be used by anyone desiring to do so. Every effort has been made by the Institute to assure the accuracy and reliability of the data contained in them; however, the Institute makes no representation, warranty, or guarantee in connection with this publication and hereby expressly disclaims any liability of responsibility for loss or damage resulting from its use or for the violation of any federal, state, or municipal regulation with which this publication might conflict.

ACKNOWLEDGMENTS

The author would like to acknowledge the following individuals for their contributions of time and expertise during this study and in the preparation of this report:

API STAFF CONTACT

Harley Hopkins, Regulatory Analysis and Scientific Affairs Department (RASA)

MEMBERS OF THE API SOIL AND GROUNDWATER TECHNICAL TASK FORCE

Curtis Stanley, Shell Global Solutions; Chairman

Appreciation is extended to Victor Kremesec, BP plc; Ravi Kolhatkar, BP plc; and Tom Henson, ExxonMobil, for their discussions, review and comments on this work. A special acknowledgment is extended to Mark Adamski, BP plc, for many discussions, ideas and data that have been incorporated in this manuscript, including the example application presented in Section 4.4. Andrew Kirkman (RETEC) is acknowledged for contributing to the review of the spreadsheet models.

PREFACE

This manuscript is presented as a supplement to API Publication Number 4682, *Free-Product Recovery of Petroleum Hydrocarbon Liquids*, which was published in June 1999. Model scenarios are described for free-product hydrocarbon liquid recovery using single- and dual-pump well systems, skimmer wells, vacuum-enhanced well systems, and trenches. Use of spreadsheet software to compute recovery rates, volumes and times is discussed, and example applications are provided. The basic modeling equations and background material are also provided.

TABLE OF CONTENTS

Section Page

LIST OF FIGURES

EXECUTIVE SUMMARY

This document addresses the application of proven technologies for recovering free-product petroleum releases to groundwater. The manuscript is a supplement to API Publication Number 4682, and documents spreadsheet models for design and analysis of liquid free-product recovery systems using single- and dual-pump wells, vacuum-enhanced wells, skimmer wells, and trenches. The principles that govern the distribution and movement of free-product petroleum hydrocarbons near the water table in an unconfined groundwater aquifer are reviewed. Models for predicting free-product recovery system performance are presented. Four spreadsheet models [LNAPL(vG-B).xls, LNAPL(vG-M).xls, LNAPL(vG-B-2L).xls, and LNAPL(vG-M-2L).xls] are described, and example applications are presented and discussed.

This manual is useful for evaluating remediation options at sites where free product is present at the water table of an unconfined aquifer or perched on a confining bed. It assumes that the reader has a basic understanding of hydrogeology and is aware of subsurface complexities (e.g., heterogeneity and water-table fluctuation) that complicate estimates of free-product recovery. Background material is presented in API Publication No. 4682, including a description of remediation technologies associated with free-product recovery, physical/chemical parameters that are essential in the design and analysis of free-product recovery systems, and information and data for parameter estimation.

The most significant changes from API Publication No. 4682 that are included in the present model formulation are a focus on the van Genuchten representation for soil retention of fluid, and use of piece-wise linear equations to relate both the LNAPL specific volume and relative permeability functions to the monitoring-well thickness of the LNAPL layer. The explicit representation of the LNAPL-layer relative permeability function results in model predictions that differ most significantly from the previous model when the Mualem relative permeability model is selected. The capability for addressing the transient performance of skimmer wells and trench systems has been added. In addition, a simple case of aquifer heterogeneity with layers of different soil texture properties can be analyzed.

SECTION 1 – INTRODUCTION

1.1 Background and Objectives

The American Petroleum Institute (API) Publication Number 4682, *Free-Product Recovery of Petroleum Hydrocarbon Liquids* (Charbeneau et al., 1999), provides an overview of recovery technologies for petroleum hydrocarbon liquids that are released to the subsurface environment and accumulate near the water table. The primary recovery technologies include skimmer wells that produce hydrocarbon liquids and single- and dual-pump wells that produce both water and hydrocarbon liquids. Hydrocarbon liquid recovery rates may also be enhanced by applying a vacuum pressure to the well to increase the gradient towards the well within the hydrocarbon layer. API 4682 describes two (Excel spreadsheet) models that may be used to characterize the subsurface distribution and mobility of liquid hydrocarbon (lighter-than-water nonaqueous phase liquids, LNAPL), and to calculate the potential recovery rate and time using single- and dual-pump wells, and vacuum-enhanced wells.

The present manuscript is a supplement to API 4682 that describes additional work that was funded through API and supported by its Soil and Groundwater Technical Task Force. The manuscript describes a more general modeling framework for characterization of subsurface LNAPL distribution using the capillary pressure head-saturation model of van Genuchten (1980), and for describing the mobility and potential recovery using single- and dual-pump wells, vacuum-enhanced wells, skimmer wells and trenches. Both the LNAPL layer volume and relative permeability are described by fitting a piecewise linear model to the magnitudes calculated from vertical distributions of hydrocarbon saturation and relative permeability based on the assumption of vertical equilibrium (the valid range for this assumption is discussed in API 4682). The models presented in Appendix A also simulate a simple case of soil heterogeneity with an abrupt vertical change in soil texture, where the upper and lower layers may have differing soil characteristics.

1.2 Senarios for Free-Product Hydrocarbon Liquid Recovery

Proven technologies for free-product recovery of petroleum hydrocarbon liquids are described in API 4682. Models to provide quantitative estimates of system performance must necessarily be based on simplifying assumptions that will not be applicable to all field conditions. Nevertheless, the models provide insight and guidance that should be helpful in technology selection and system design, and in analysis of system performance. The model scenarios for well systems and trenches are discussed separately.

The subsurface porous media is assumed to be homogeneous, as shown in Figure 1.1. [A simple case of aquifer heterogeneity where a soil layer of one texture overlies a layer with a differing texture, with an abrupt horizontal interface separating the layers, is presented in Appendix A.] Figure 1.1 shows a monitoring well with an LNAPL layer located between the air-NAPL interface z_{ao} and the NAPL-water interface z_{ow}. The total monitoring well LNAPL thickness is b_o. The elevation of the water table, z_{aw}, provides the datum for fluid levels. While the water table is not present because of the LNAPL layer, its elevation is easily determined from the elevations z_{ao} and z_{ow}, and the LNAPL density ρ_o.

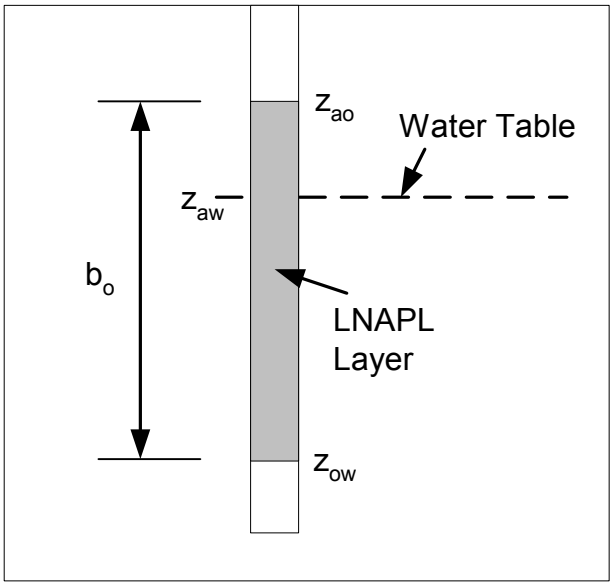

Figure 1.1. Monitoring well LNAPL thickness, b_o

The texture characteristics that must be defined for the porous media include the porosity *n*; the van Genuchten parameters *N* and α; and the irreducible water saturation, S_{wr}; and residual LNAPL saturation values for the vadose zone and saturated zone, S_{orv} and S_{ors}. Fluid properties include the LNAPL density, ρ_o (it is assumed that the water density is 1 g/cm^3), and the water and LNAPL surface and interfacial tensions, σ_{aw}, σ_{ao}, and σ_{ow}.

1.2.1. Scenarios for Recovery Well Systems

The basic scenario for free-product recovery using well systems is the same for single- and dual-pump wells, vacuum-enhanced wells, and skimmer wells. The performance of each well is characterized in terms of its radius of capture R_c, with a typical scenario shown in Figure 1.2. This figure depicts a plan view of an LNAPL lens (in gray color) with 11 recovery wells located so that the pattern of wells with their radius of capture will cover the area of the lens. For single- and dual-pump well systems, the radius of capture could extend out to the radius of influence (water production) of the well. For vacuum-enhanced systems, the radius of influence of the vacuum extraction well (which is typically on the order of 30 – 40 feet) limits the radius of capture. For

skimmer wells, the radius of capture is limited to a greater but unknown extent, which is probably on the order of 10 – 20 feet.

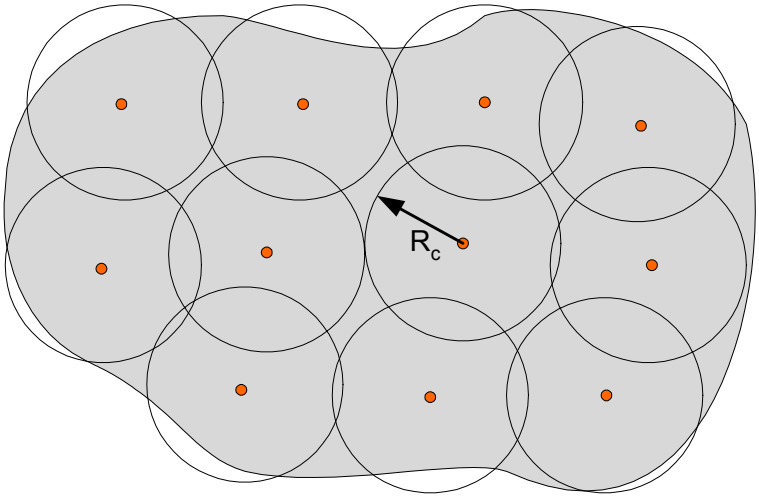

Figure 1.2. Recovery well system with 11 recovery wells showing the radius of capture

The data required for analysis of recovery-well-system performance includes the radius of capture for the well, the LNAPL viscosity (the water viscosity is assumed to be 1 cp), and water production rate for a water-enhanced system or wellhead vacuum pressure for a vapor-enhanced system. For a water-enhanced system, the effective depth of penetration of the well into the aquifer must be specified, while for a vacuum-enhanced system, the screened interval of the vadose zone must be given along with the effective relative permeability of the vadose zone (due to the presence of soil water, the permeability of the vadose zone may be reduced from its air-saturated value). If zero water production and wellhead pressure are specified, then the well is assumed to function as a skimmer well.

1.2.2. Scenario for LNAPL Recovery Using Trenches

The modeling framework may also be used to represent a simple trench recovery system, such as shown in Figure 1.3. The trench has a width W_T transverse to the direction of groundwater flow. The LNAPL lens is of length L_T in the direction of groundwater flow, and width W_T. The natural groundwater hydraulic gradient J_w is transferred to the floating LNAPL layer, and carries it into the trench where LNAPL is

removed by skimmer wells or other technology. The rate of LNAPL discharge into the trench will depend on the effective lens thickness as observed in a monitoring well, soil texture characteristics, the natural groundwater hydraulic gradient, and whether groundwater is also produced from the trench in order to increase the hydraulic gradient. If the trench cuts across an LNAPL lens, then the upstream and downstream sections of the lens must be analyzed separately, with J_w being negative on the downstream side.

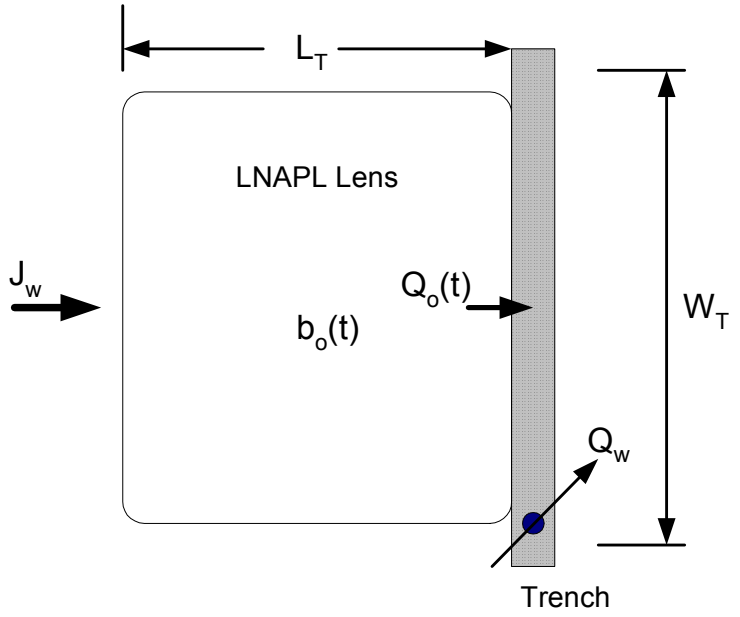

Figure 1.3. Simple Trench System for LNAPL Recovery

1.3. Overview

The models for well and trench recovery systems provide estimates of the recovery volume and rate as a function of time. The mathematical models on which these estimates are based use a simple representation of the LNAPL layer effective saturation and permeability. However, the representation is consistent with the actual formation distributions of LNAPL saturation and relative permeability under conditions of vertical equilibrium, so that "continuity" is maintained within the modeling framework. These representations are described in Section 2, which describes the saturation distribution based on the van Genuchten (1980) capillary pressure model and conditions

of vertical equilibrium. This model was not described in API 4682, which focused on application of the Brooks and Corey (1964) power law model for representing the soil characteristics. The LNAPL layer relative permeability distribution is also described, using both the Burdine (1953) and Mualem (1976) models to relate saturation and relative permeability.

The mathematical models for predicting free-product recovery are developed in Section 3. These models are based on the free-product thickness that one would observe in a monitoring well that was in good communication with the formation fluids (water, LNAPL, air). The rate equations for single- and dual-pump wells, vacuum-enhanced wells, skimmer wells, and trench recovery systems depend on the monitoring well LNAPL thickness and on the discharge of formation fluids (water or air). The principle of continuity is applied to predict how the monitoring well LNAPL thickness (and recovery rate) varies as a function of time. Section 4 presents a series of examples that describe features of the model implementation and model application.

Appendix A describes an extended version of the model that addresses a simple case of aquifer heterogeneity, with two layers having different soil texture characteristics. Calculation of effective layer specific volume and relative permeability are described for this two-layer case, and extension of the time-variable recovery models are presented. Example applications are also provided.

Appendix B provides a listing of the Visual Basic function calls that are used in the spreadsheets. Appendix C provides representative van Genuchten model soil retention parameter values for different soil texture classes. Tables of representitive fluid properties can be found in Appendix D. Appendix E contains porosity and residual saturation values from the literature.

SECTION 2 – LNAPL SATURATION AND RELATIVE PERMEABILITY DISTRIBUTIONS

This section describes the vertical distribution of fluid saturation and relative permeability for a homogeneous porous media. The resulting relationships are used to develop simple representations of effective specific volume and relative permeability for an LNAPL lens.

2.1 NAPL Saturation Distribution

This subsection first considers the capillary pressure scaling relationships for different fluid systems, and then the consequences of vertical equilibrium for describing capillary pressure distributions are discussed. Results are used to estimate the saturation distribution for homogenous porous media.

2.1.1 Capillary Pressure Scaling Relationships

According to the van Genuchten (1980) model, the water saturation S_w is related to the suction pressure head h through

$$S_w(h) = S_{wr} + (1 - S_{wr})\left[\frac{1}{1 + (\alpha h)^N}\right]^M \qquad (2.1)$$

In equation 2.1, S_{wr} is the irreducible (residual) water saturation and α, N and M are model parameters (where $M = 1 - 1/N$; $N = 1/(1-M)$). The parameter α is for the air-water fluid system, and its magnitude is inversely related to the thickness of the capillary fringe. The Brooks and Corey (1964) displacement pressure head (Ψ_b) is related to α through the approximate relation $\alpha \sim 1/\Psi_b$. The parameter N is proportional to the pore-size distribution index (λ) of Brooks and Corey, where roughly one has $N = \lambda + 1$. Representative values for a sand soil are $S_{wr} = 0.15$, $\alpha = 2.0$ ft^{-1} and $N = 4.0$. The resulting soil characteristic curve is shown in Figure 2.1.

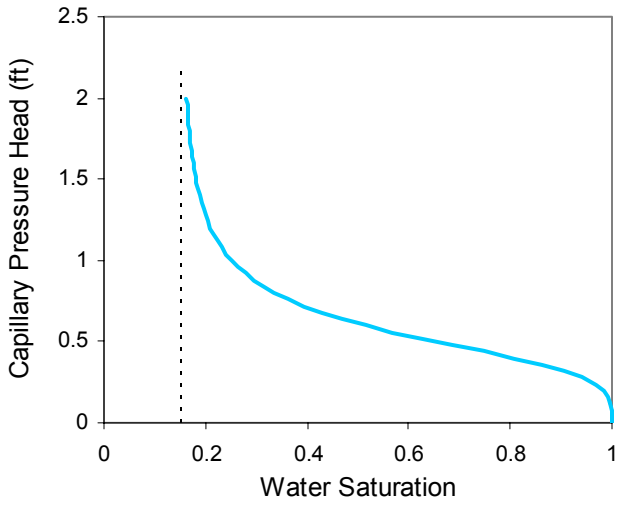

Figure 2.1. Representative soil characteristic curve based on the van Genuchten model with S_{wr} = 0.15, α = 2.0 ft^{-1}, and N = 4.0

Equation 2.1 may be used for other fluid combinations if appropriate scaling relationships are introduced. It is assumed that water is the wetting fluid, air the nonwetting fluid, and that LNAPL has intermediate wettability. For the three-phase (water, LNAPL, air) system, Leverett's (1941) assumption is that the water saturation is a function of the LNAPL-water capillary pressure, while the total liquid saturation (water plus LNAPL) is a function of the air-LNAPL capillary pressure.

The introduction of scaling relationships are based on Laplace's equation (for capillary pressures) that relates the pressure difference across an interface between two fluid phases to the radius of curvature of this interface. For fluid phases i and j, this equation may be written

$$\frac{p_{cij}}{\sigma_{ij}} = \frac{2}{r_c} \qquad (2.2)$$

In equation 2.2, p_{cij} is the capillary pressure (pressure in the nonwetting phase *i* minus the pressure in the wetting phase *j*), σ_{ij} is the surface or interfacial tension between phases *i* and *j*, and r_c is the radius of curvature of the interface that separates these phases. The reasoning behind the scaling relationships is as follows. The right side of equation 2.2 should be determined by the distribution of pores within the porous medium and should be directly related to the fluid saturation (with the wetting phase

occupying the smaller pore sequences). A decrease in the radius of curvature would correspond to the interface moving into pores of smaller size with larger capillary pressure. This would correspond to a decrease in wetting phase saturation. [This does not reflect hysteresis, wherein the sequence of filled pores is different upon drainage and imbibition.] The left side of equation 2.2 can be scaled for different fluid combinations.

For fluid combination *i-j*, the capillary pressure head parameter α may be scaled following Leverett (1941):

$$\alpha_{ij} = \left(\frac{\rho_j - \rho_i}{\rho_w - \rho_a}\right)\left(\frac{\sigma_{aw}}{\sigma_{ij}}\right)\alpha \qquad (2.3)$$

In equation 2.3 the term containing the fluid density values appears because capillary pressure head values are being scaled rather than capillary pressures. At standard atmospheric pressure and a temperature of 20^o C, the air density is 0.0012 g/cm^3 and is usually neglected compared with the water density of 1 g/cm^3. Thus, for scaling the capillary pressure head between LNAPL and water, equation 2.3 becomes

$$\alpha_{ow} = \left(\frac{\rho_w - \rho_o}{\rho_w}\right)\left(\frac{\sigma_{aw}}{\sigma_{ow}}\right)\alpha = \left(1 - \rho_r\right)\left(\frac{\sigma_{aw}}{\sigma_{ow}}\right)\alpha \qquad (2.4)$$

In equation 2.4, ρ_r is the LNAPL/water density ratio, or the LNAPL specific gravity. Similarly, in scaling the capillary pressure heads between air and LNAPL, equation 2.3 takes the form

$$\alpha_{ao} = \rho_r\left(\frac{\sigma_{aw}}{\sigma_{ao}}\right)\alpha \qquad (2.5)$$

Equations 2.4 and 2.5 provide the appropriate scaling relationships.

2.1.2 Vertical Equilibrium

Use of equation 2.1 and appropriately scaled capillary pressure relations to describe the vertical distribution of fluid saturation requires the assumption of vertical equilibrium, wherein the pressure in each phase satisfies the hydrostatic pressure equation. To help develop ideas, consider the LNAPL-water system. The hydrostatic

pressure equation for the LNAPL and water phase take the following form for an incompressible fluid.

$$p_o(z) = p_o(z^*) - \rho_o\, g\,(z - z^*)$$
$$p_w(z) = p_w(z^*) - \rho_w\, g\,(z - z^*) \tag{2.6}$$

In equation 2.6, z^* is a reference elevation that will be selected based on the following discussion. The capillary pressure is the pressure difference between the nonwetting and wetting phases (for this case this is designated as p_{cow}), and thus the capillary pressure distribution between LNAPL and water under conditions of vertical equilibrium is given by

$$p_{\text{cow}}(z) = p_{\text{cow}}(z^*) + (\rho_w - \rho_o)\, g\,(z - z^*) \tag{2.7}$$

It is most useful to select a reference elevation where the capillary pressure vanishes, that is, the pressure in the nonwetting and wetting phases are the same. From equation 2.2, this would require that the radius of curvature of the interface between the phases be large (infinite). This would be the case of a monitoring well in equilibrium with formation fluids, and with reference to Figure 1.1, the elevation $z^* = z_{ow}$ serves as the appropriate datum. Thus the capillary pressure head distribution under conditions of vertical equilibrium may be specified by

$$h_{\text{ow}} = \frac{p_{\text{cow}}}{(\rho_w - \rho_o) g} = z - z_{\text{ow}} \tag{2.8}$$

To show consistency of the scaling relationships for equation 2.1 note that

$$\alpha_{\text{ow}}\, h_{\text{ow}} = \left(\frac{\rho_w - \rho_o}{\rho_w}\right)\left(\frac{\sigma_{\text{aw}}}{\sigma_{\text{ow}}}\right)\alpha \times \frac{p_{\text{cow}}}{(\rho_w - \rho_o) g} = \alpha\, h \tag{2.9}$$

The last step in equation 2.9 follows from equation 2.2, according to which, $p_{cow}/\sigma_{ow} = p_{caw}/\sigma_{aw} = p_c/\sigma$, and $h = p_c/(\square_w\, g)$.

In a similar fashion to equation 2.8, for the air-LNAPL system one finds

$$h_{\text{ao}} = z - z_{\text{ao}} \tag{2.10}$$

In equation 2.10, z_{ao} is the elevation of the air-LNAPL interface in a monitoring well, as shown in Figure 1.1. Finally, using similar arguments for the water phase we have

$$h \equiv h_{aw} = z - z_{aw} \tag{2.11}$$

Together, equations 2.8, 2.10 and 2.11 allow one to calculate the pressure distribution within any phase under conditions of vertical equilibrium. For all developments below, the water table is the elevation datum, and $z_{aw} = 0$. Other elevations are referenced to this datum.

2.1.3 LNAPL and Water Saturation Distribution

Equation 2.1 may be written as

$$\Theta_w(h) = \left(\frac{S_w(h) - S_{wr}}{1 - S_{wr}} \right) = \left[\frac{1}{1 + (\alpha h)^N} \right]^M \tag{2.12}$$

In equation 2.12, Θ_w is the air-water reduced saturation, and it scales the water saturation to range between values of 0 and 1. In order to apply this equation to other fluid-phase pairs, the appropriate reduced saturation functions must be identified, which also must have values that scale to range from 0 to 1. Using the Leverett assumptions for the LNAPL-water pair, along with equations 2.8 and 2.4 for vertical equilibrium and capillary scaling, the water saturation distribution may be represented by the following equation:

$$S_w(z) = S_{wr} + (1 - S_{wr} - S_{ors}) \left[\frac{1}{1 + (\alpha_{ow}(z - z_{ow}))^N} \right]^M \tag{2.13}$$

In equation 2.13, S_{ors} is the residual LNAPL saturation in the saturated zone and z_{ow} is the elevation of the LNAPL-water interface in a monitoring well. In a similar fashion, for the total liquid (water plus LNAPL)-air saturation distribution, equation 2.12 becomes

$$S_t(z) = S_{wr} + S_{orv} + (1 - S_{wr} - S_{orv}) \left[\frac{1}{1 + (\alpha_{ao}(z - z_{ao}))^N} \right]^M \tag{2.14}$$

In equation 2.14, $S_t(z) = S_w(z) + S_o(z)$, S_{orv} is the residual LNAPL saturation in the vadose zone, and z_{ao} is the elevation of the air-LNAPL interface in a monitoring well. For elevation $z < z_{ao}$, all of the pore space is filled with liquid (water plus LNAPL), so $S_t = 1$. Likewise, for elevation $z < z_{ow}$, all of the pore space is filled with water plus residual LNAPL (if any is present), so $S_w = 1 - S_{ors}$.

Given equations 2.13 and 2.14, the LNAPL distribution may be found from

$$S_o(z) = S_t(z) - S_w(z) \qquad (2.15)$$

Equation 2.15 predicts the total saturation of LNAPL, and does not reflect the fact that a fraction of this LNAPL phase will remain trapped within the saturated and vadose zones (given by the values of S_{ors} and S_{orv}, respectively).

Figure 2.2 shows the LNAPL saturation distribution corresponding to a monitoring-well LNAPL thickness $b_o = 2.0$ feet, for a soil with same texture properties used in Figure 2.1. The horizontal dashed line marks the elevation of the water table. The box on the right side shows the monitoring-well LNAPL thickness. The LNAPL curve shows the free-product LNAPL saturation distribution, as predicted using equations 2.13 to 2.15. The dashed curve on the left side of the figure marks the residual LNAPL distribution. For this case, residual LNAPL extends above and below the free-product LNAPL layer. The extension of the residual LNAPL distribution within the free-product layer shows the saturation distribution that would become immobile as LNAPL is recovered. However, all LNAPL within the free-product layer is considered mobile. Capillary forces trap LNAPL only as the LNAPL saturation is reduced.

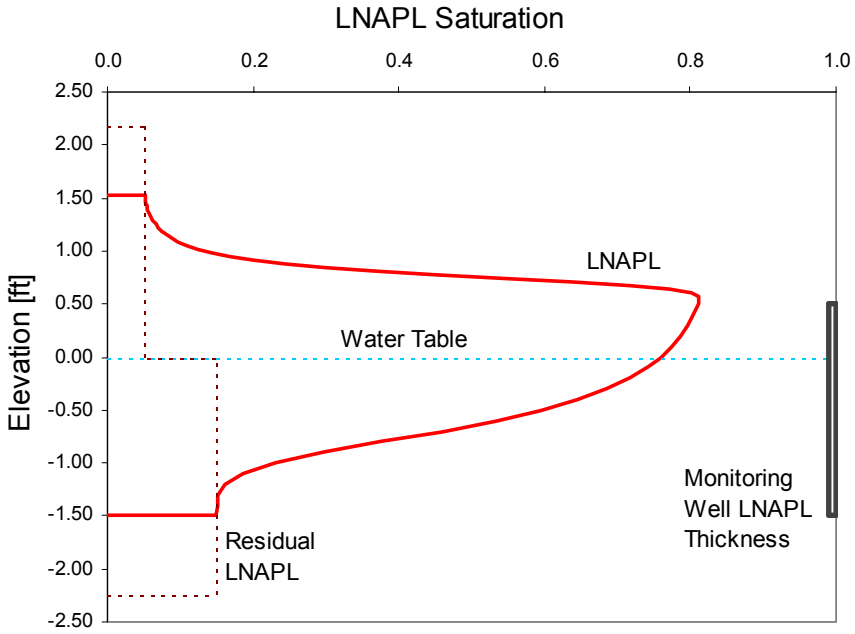

Figure 2.2. LNAPL saturation distribution

The maximum elevation of free-LNAPL (LNAPL saturation greater than residual) is found by setting $S_o(z) = S_{orv}$ in equation 2.15 and solving for $z = z_{max}$. This leads to the equation

$$A - 1 = \left[\alpha_{ao}\left(z - z_{ao}\right)\right]^N - A\left[\alpha_{ow}\left(z - z_{ow}\right)\right]^N \tag{2.16}$$

In equation 2.16,

$$A = \left(\frac{1 - S_{wr} - S_{orv}}{1 - S_{wr} - S_{ors}}\right)^{1/M} \tag{2.17}$$

In general, equation 2.16 must be solved iteratively for $z = z_{max}$. However, in the special case where $S_{orv} = S_{ors}$ one finds $A = 1$ and

$$z = z_{max}^{\ *} = \frac{\alpha_{ao} z_{ao} - \alpha_{ow} z_{ow}}{\alpha_{ao} - \alpha_{ow}} \tag{2.18}$$

However, z_{ao} and z_{ow} are related to the LNAPL layer thickness in a monitoring well, b_o, through

$$z_{aw} - z_{ow} = \rho_r b_o \tag{2.19}$$

$$z_{ao} - z_{aw} = \left(1 - \rho_r\right) b_o \tag{2.20}$$

In equations 2.19 and 2.20, ρ_r is the LNAPL specific gravity. Selecting z_{aw} as the datum ($z_{aw} = 0$), equation 2.18 may be reduced to the form

$$z_{\max}^{*} = \left[\frac{(\sigma_{ao} + \sigma_{ow})(1 - \rho_r)}{\rho_r \sigma_{ow} - (1 - \rho_r)\sigma_{ao}} \right] \rho_r b_o \qquad (2.21)$$

Equation 2.21 leads to the following model-specific requirement between the surface and interfacial tensions, and the specific gravity:

$$\sigma_{ow} > \frac{1 - \rho_r}{\rho_r} \sigma_{ao} \qquad (2.22)$$

The LNAPL capillary-rise increases indefinitely as the limit in equation 2.22 is approached. Examination of the resulting LNAPL distributions as this limit is approached shows that the limiting condition corresponds to infinite capillary rise of an LNAPL film (infinitely small saturation above residual), presumably associated with a positive spreading coefficient against the pull of gravity. These small saturation values do not significantly impact the effective LNAPL-layer specific volume and relative permeability, and thus they may be ignored in issues of free-product recovery. However, if the conditions specified by equation 2.22 do not hold, then an algorithm based on solution of equation 2.16 for the maximum elevation of free-LNAPL cannot be used.

Field data show measured surface and interfacial tension values that do not satisfy equation 2.22. An alternative algorithm for estimating the effective capillary rise is to work directly with equation 2.15 and search with increasing elevation for the condition where

$$S_o(z) - S_{orv} \leq \varepsilon \qquad (2.23)$$

In equation 2.23, ε is a sufficiently small value (say 0.001) and the elevation that first satisfies this equation is taken as z_{max}.

Equations 2.13, 2.14 and 2.15 may be used to find the LNAPL saturation distribution within the groundwater formation corresponding to a given monitoring well LNAPL thickness under conditions of vertical equilibrium. Figure 2.3 shows the LNAPL saturation distribution for the soil characteristic curve of Figure 2.1 corresponding to a monitoring well LNAPL thickness value of b_o = 2.0 feet with ρ_r = 0.75, S_{orv} = 0.05, S_{ors} =

0.15, and σ_{ao} = 25 dyne/cm. The horizontal dashed line shows the elevation of the water table, and the largest LNAPL saturation values occur within the upper part of the water table capillary fringe. The two curves that are shown differ in values of σ_{ow}, with the curve with greater capillary rise having σ_{ow} = 5 dyne/cm compared with 25 dyne/cm for the other curve. From this figure it is seen that the most significant effect of increasing σ_{ow} values is to decrease the LNAPL saturation below the water table and within the capillary fringe. There is also a increase in the LNAPL capillary rise, though it does not result in a large increase in LNAPL saturation above residual at locations above the water table.

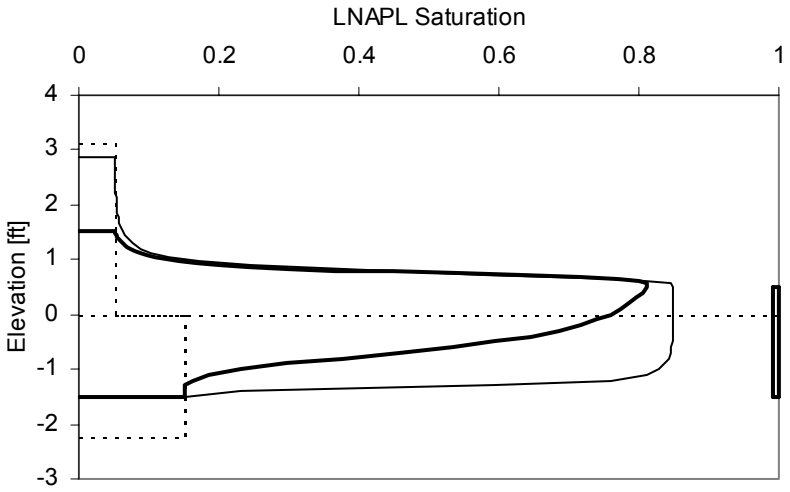

Figure 2.3. Influence of interfacial tension on LNAPL distribution based on the soil characteristic curve of Figure 2.1. The thin curve with greater capillary rise has σ_{ow} = 5 dyne/cm, while the thick curve corresponds to σ_{ow} = 25 dyne/cm and is the same distribution as shown in Figure 2.2.

Figure 2.4 shows the LNAPL saturation distribution for monitoring well LNAPL thickness values of b_o = 3, 2, 1, and 0.5 feet, for the condition with σ_{ow} = 25 dyne/cm and other parameters as shown in Figures 2.1 to 2.3. The significant decrease in "free-product" with decreasing b_o is apparent.

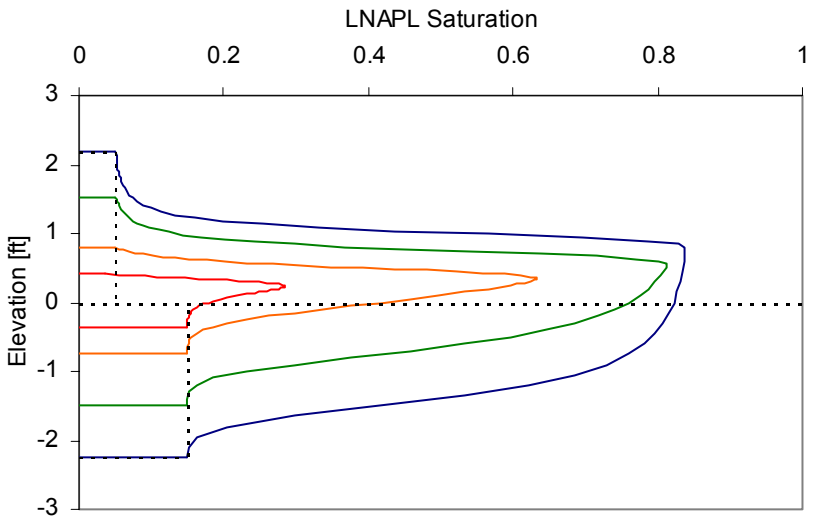

Figure 2.4. LNAPL distribution as a function of monitoring well LNAPL thickness, b_o. Distributions correspond to values b_o = 3, 2, 1, and 0.5 feet. The dashed vertical lines above and below the water table correspond to residual LNAPL values S_{orv} = 0.05 and S_{ors} = 0.15. It is saturation values in excess of these that are considered recoverable.

2.1.4 LNAPL-Layer Specific Volume, D_o

A measure of great interest in efforts to quantify free product is the relationship between the monitoring well LNAPL thickness, b_o, and the specific free-product volume (volume of LNAPL per unit surface area). The specific free-product volume, D_o, may be calculated from

$$D_o(b_o) = \int_{z_{ow}}^{z_{max}} n\, S_o(z)\, dz \qquad (2.24)$$

The function $D_o(b_o)$ tends to be well-behaved and may be approximated piecewise by a linear function of the form

$$D_o = \beta\,(b_o - \chi) \qquad (2.25)$$

Figure 2.5 shows the "specific storage" function $D_o(b_o)$ for the two parameter sets used to develop Figure 2.3. For each parameter set, the solid curves show the calculated function while the dashed line segments show the piecewise linear fit with three segments. It is difficult to distinguish the solid and dashed curves, showing that a three-segment linear model provides an adequate fit to equation 2.24 for the parameter sets, and this is generally thought to be the case.

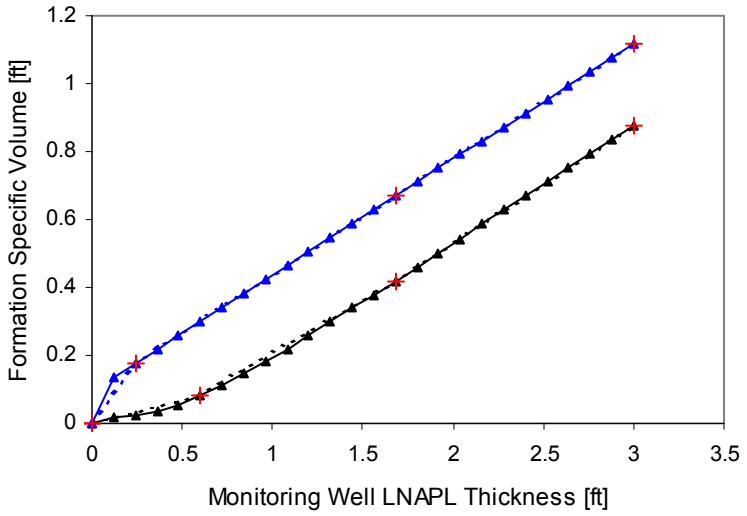

Figure 2.5. Formation specific volume function, $D_o(b_o)$. The lower curve corresponds to the condition with σ_{ow} = 25 dyne/cm in Figure 2.3, while the upper curve corresponds to σ_{ow} = 5 dyne/cm.

2.2 LNAPL-Layer Relative Permeability

The vertical distribution of water and LNAPL saturation may be used to estimate the vertical distribution of LNAPL relative permeability, which in turn may be used to assess LNAPL mobility and potential recovery rates. Methods for relating LNAPL saturation-capillary pressure to relative permeability are based on models of pore size distribution and association of permeability to various pore sizes occupied by LNAPL. One issue that arises concerns identification of the appropriate value for residual LNAPL saturation; the same model is used both above and below the water table, and selection of S_{orv} or S_{ors} is uncertain. A decision was made to set the residual LNAPL value to zero during application of the relative permeability models. This decision results in the following model equations.

Using a three-phase integration of the Burdine (1953) equations with the Brooks and Corey (1964) soil characteristic model (power-law model), the LNAPL relative permeability may be calculated from

$$k_{ro}\left(S_w, S_o\right) = S_o^{\,2}\left[\left(\frac{S_t - S_{wr}}{1 - S_{wr}}\right)^{\frac{\lambda+2}{\lambda}} - \left(\frac{S_w - S_{wr}}{1 - S_{wr}}\right)^{\frac{\lambda+2}{\lambda}}\right] \qquad (2.26)$$

In equation 2.26, S_t is the total liquid saturation (S_o + S_w), and λ is the pore size distribution index. The pore size distribution index may be estimated from van Genuchten model parameters using (Lenhard et al., 1989)

$$\lambda = \frac{M}{1-M}\left(1-0.5^{1/M}\right) \tag{2.27}$$

Similarly, a three-phase integration of the Mualem (1976) equation with van Genuchten's soil characteristics function (Parker et al., 1987) gives

$$k_{\mathrm{ro}}\left(S_w, S_o\right) = S_o^{1/2}\left\{\left[1-\left(\frac{S_w - S_{\mathrm{wr}}}{1-S_{\mathrm{wr}}}\right)^{1/M}\right]^{M} - \left[1-\left(\frac{S_t - S_{\mathrm{wr}}}{1-S_{\mathrm{wr}}}\right)^{1/M}\right]^{M}\right\}^{2} \tag{2.28}$$

In equations 2.26 and 2.28, the leading term accounts for tortuosity while the second term within brackets accounts for LNAPL-occupancy of pores within a given range.

Equations 2.26 and 2.28 predict different distributions of LNAPL relative permeability for the same set of fluid saturation values, with equation 2.28 generally predicting larger values for LNAPL relative permeability. For example, Figure 2.6 compares the LNAPL saturation distribution of Figure 2.2 (with σ_{ow} = 25 dynes/cm) with the case with S_{orv} = S_{ors} = 0. In the former case the value of z_{max} is 1.53 feet, while in the latter, z_{max} = 1.47 feet (for comparison, z_{max}* = 1.50 feet from equation 2.21). This figure suggests that setting S_{orv} = S_{ors} = 0 does not significantly effect the values of LNAPL saturation throughout most of the lens thickness. The corresponding effect on the effective lens relative permeability should also be minor because the relative permeability associated with small LNAPL saturation values (where the difference between the two curves is largest) is small.

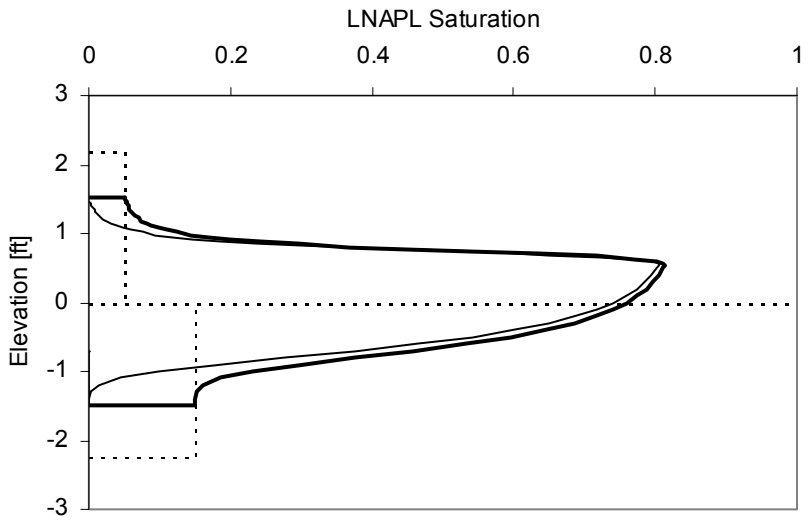

Figure 2.6. LNAPL saturation distribution in soil with properties from Figure 2.2 for b_o = 2 feet. The two curves correspond to S_{orv} = 0.05, S_{ors} = 0.15, and S_{orv} = S_{ors} = 0.

Figure 2.7 shows the LNAPL relative permeability distribution predicted by equations 2.26 and 2.28 for the LNAPL saturation distribution of Figure 2.6 (with zero residual saturation values). The solid curve is the Burdine model while the dashed curve corresponds to Mualem's model. Mualem's model predicts larger relative permeability values.

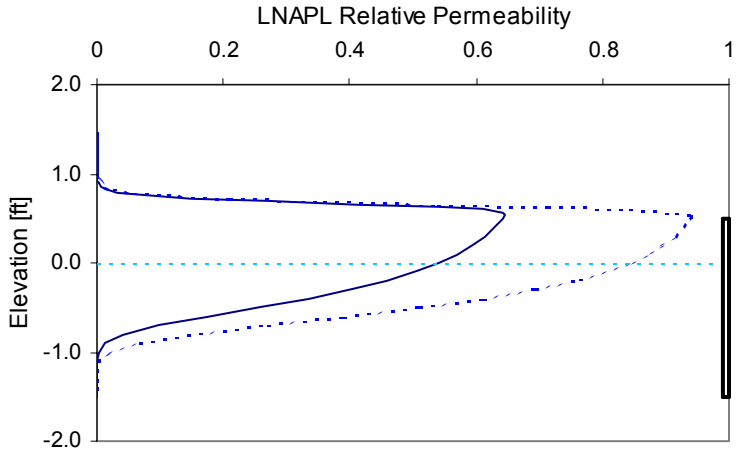

Figure 2.7. LNAPL relative permeability distribution predicted by the Burdine (equation 2.26; solid line) and Mualem (equation 2.28; dashed line) models, corresponding to the LNAPL saturation distribution shown in Figure 2.6 with zero residual saturation values.

For the LNAPL relative permeability distributions predicted by using equations 2.13, 2.14 and 2.15 [with S_{orv} = S_{ors} = 0] with either equation 2.26 or 2.28, a variable of interest is the effective relative permeability of the LNAPL layer. This may be calculated from

$$\bar{k}_{\mathrm{ro}}(b_o) = \frac{1}{b_o}\int_{z_{\mathrm{ow}}}^{z_{\max}} k_{\mathrm{ro}}\left(S_w(z), S_o(z)\right) dz \tag{2.29}$$

While equation 2.29 cannot be evaluated analytically, it is well behaved and can be approximated using a piecewise linear function of the form

$$\bar{k}_{\mathrm{ro}} = \eta(b_o - \xi) \tag{2.30}$$

Figure 2.8 shows the LNAPL-layer relative permeability function $\bar{k}_{\mathrm{ro}}(b_o)$ for the two relative permeability models. As expected, the Mualem model has larger permeability values for a given LNAPL-layer thickness. Also shown in the figure are the piecewise linear approximations, with three segments in each case.

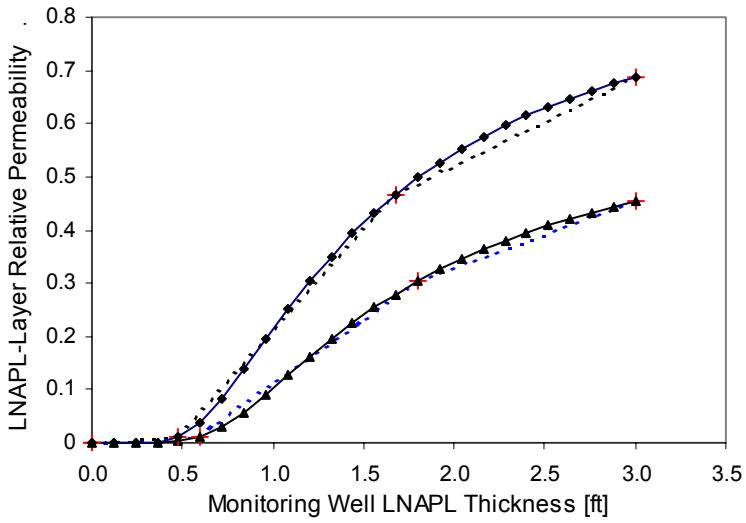

Figure 2.8. LNAPL-layer relative permeability functions $\bar{k}_{ro}(b_o)$ for the models of Mualem (upper curve) and Burdine (lower curve). The dashed curves show the piecewise linear fit model representation.

SECTION 3 – MODELS FOR LIQUID FREE-PRODUCT RECOVERY

In modeling LNAPL recovery using wells or trenches for conditions of vertical equilibrium, both the specific volume and LNAPL-layer relative permeability may be represented as piecewise linear functions of the monitoring well LNAPL thickness. These representations are expressed in equations 2.25 and 2.30, and Figures 2.5 and 2.8 suggest that the layer functions may be adequately fit using a three-segment model. These representations allow development of relatively simple models for predicting the performance of free-product recovery systems. This section presents the basic equations for well systems and for trenches.

3.1 Free-Product Recovery Using Well Systems

For single- and dual-pump wells, and for vacuum-enhanced well systems, production of water or air creates the hydraulic gradient that is responsible for LNAPL migration to the recovery well. For skimmer wells, the LNAPL drawdown at the well creates the gradient, and a different rate equation is followed. Rate equations are combined with continuity and specific retention parameters for the LNAPL layer to develop performance equations for the recovery system.

3.1.1 Rate Equations for LNAPL Recovery

Under conditions where the LNAPL recovery rate is determined by water production, the water and LNAPL discharge are related through (see Charbeneau et al., 1999, Charbeneau et al., 2000)

$$Q_o = \frac{\rho_o \mu_w \bar{k}_{\mathrm{ro}} Q_w b_o}{\rho_w \mu_o b_w} \equiv \frac{\rho_r \bar{k}_{\mathrm{ro}} Q_w b_o}{\mu_r b_w} \tag{3.1}$$

In equation 3.1 μ_r is the LNAPL/water viscosity ratio and b_w is the effective thickness of the aquifer, which in the case of a thick formation, is determined by the length of well screen. Similarly, when LNAPL recovery is determined through airflow (vacuum-enhanced recovery), the air and LNAPL discharge are related through

$$Q_o = \frac{\rho_o \mu_a \bar{k}_{\mathrm{ro}} Q_a b_o}{\rho_w \mu_o \bar{k}_{\mathrm{ra}} L_w} \equiv \frac{\rho_r \mu_a \bar{k}_{\mathrm{ro}} Q_a b_o}{\mu_o \bar{k}_{\mathrm{ra}} L_w} \tag{3.2}$$

In equation 3.2, μ_a is the dynamic viscosity of air (which is assumed to be 0.018 cp), Q_a is the air discharge, $\bar{k}_{\mathrm{ra}}$ is the average relative permeability of the vadose zone, and L_w is the length of well screen in the vadose zone for airflow.

The rate equation for a skimmer well was developed by Dr. Russell Johns (see Johns et al., 2003). The LNAPL discharge is given by

$$Q_o = \frac{\pi(\rho_w - \rho_o)\rho_o \mu_w K_w \bar{k}_{\mathrm{ro}} b_o^{\,2}}{\rho_w^{\,2} \mu_o \ln(R/r_w)} \equiv \frac{\pi(1-\rho_r)\rho_r K_w \bar{k}_{\mathrm{ro}} b_o^{\,2}}{\mu_r \ln(R/r_w)} \tag{3.3}$$

In equation (3.3), K_w is the hydraulic conductivity of the formation, R is the radius of influence of the skimmer well, and r_w is the skimmer well radius.

In LNAPL recovery, one may apply water and vacuum enhancement to increase the recovery rate, so that equations 3.1 and 3.2 may be added. The skimmer well equation 3.3 reflects LNAPL recovery without any enhancement of the rate, and thus it stands alone.

3.1.2 LNAPL-Layer "Specific Retention"

Within a radius of capture, R_c, the total LNAPL free-product volume is a function of the monitoring well LNAPL thickness:

$$V_o(b_o) = \pi R_c^{\,2} D_o(b_o) = \pi R_c^{\,2} \beta(b_o - \chi) \tag{3.4}$$

Not all of this volume can be recovered through liquid free-product recovery technologies because of residual saturations that exist within the vadose zone and saturated zone as the LNAPL thickness is reduced. If the monitoring well LNAPL thickness was reduced to zero, the remaining residual LNAPL volume within the zone of recovery may be calculated as

$$V_{\mathrm{or}}(t) = \pi R_c^{\,2} [(1-\rho_r) n S_{\mathrm{orv}} + \rho_r n S_{\mathrm{ors}}] b_o(t) \tag{3.5}$$

The difference between the volumes in equations 3.4 and 3.5 represents the recoverable free-product volume, which may be written as

$$V_o(b_o) = V_o(b_o) - V_{\mathrm{or}}(b_o) = \pi R_c^{\,2} [D_o - \gamma b_o] \tag{3.6}$$

In equation 3.6,

$$\gamma = (1-\rho_r)\, n\, S_{\mathrm{orv}} + \rho_r\, n\, S_{\mathrm{ors}} \tag{3.7}$$

Equation 3.6 for the recoverable free-product volume may be written

$$V_o(b_o) = \pi R_c^{\,2}(\beta - \gamma)\, b_o - \left(\pi R_c^{\,2}\beta\chi\right) \tag{3.8}$$

where the last term in equation 3.8 is a constant. The most important use of equation 3.8 is to relate changes in recoverable free-product volume to changes in monitoring well LNAPL thickness:

$$dV_o(b_o) = \pi R_c^{\,2}(\beta - \gamma)\, db_o \tag{3.9}$$

The parameter γ plays the same role in continuity for the LNAPL layer as the specific retention plays in continuity at the water table of an unconfined aquifer, as the water level rises and falls. In this regard, $(\beta - \gamma)$ plays the role of the specific yield (Charbeneau, 2000).

3.1.3 "Enhanced" LNAPL Recovery Performance Equations

The performance equations for the various LNAPL recovery technologies are based on the continuity equation for recoverable LNAPL within the region of capture, which takes the form

$$-\frac{dV_o}{dt} = Q_o \tag{3.10}$$

With equation 3.9, equation 3.10 may be written

$$\frac{db_o}{dt} = -\frac{Q_o}{\pi R_c^{\,2}(\beta - \gamma)} \tag{3.11}$$

Equation 3.11 along with the relation $Q_o(b_o)$ and initial condition $b_o(0)$ may be solved to give the monitoring well LNAPL thickness $b_o(t)$. With equations 2.30, 3.1 and 3.2, equation 3.11 gives the differential equation

$$\frac{db_o}{dt} = -A_k\,(b_o - \xi)b_o \tag{3.12}$$

In equation 3.12, the index k refers to either water or air enhancement [for both the leading coefficient may be written $(A_w + A_a)$]. Equation 3.12 may be integrated to give

$$\ln\left[\frac{(b_o(0) - \xi)b_o(t)}{(b_o(t) - \xi)b_o(0)}\right] = \xi\, A_k\, t \tag{3.13}$$

Equation 3.13 may be arranged to give

$$b_o(t) = \frac{\xi b_o(0)}{b_o(0) - [b_o(0) - \xi] e^{-\xi A_k t}} \tag{3.14}$$

Equation 3.14 is appropriate when ξ is not equal to zero (ξ must approach 0 as b_o approaches zero). For $\xi = 0$ the integral becomes

$$b_o(t) = \frac{b_o(0)}{1 + b_o(0)(A_k t)} \tag{3.15}$$

In equations 3.14 and 3.15,

$$A_w = \frac{\rho_o \mu_w \eta Q_w}{\pi R_c^{\,2} (\beta - \gamma) \rho_w \mu_o b_w} \tag{3.16}$$

$$A_a = \frac{\rho_o \mu_a \eta Q_a}{\pi R_c^{\,2} (\beta - \gamma) \rho_w \mu_o \bar{k}_{ra} L_w} \tag{3.17}$$

Equations 3.14 through 3.17 provide the performance equations for "enhanced" LNAPL recovery using single and dual-pump wells and vacuum-enhanced recovery systems.

3.1.4 Performance Equations for Skimmer Wells

When both $Q_w = 0$ and $Q_a = 0$, then the recovery well functions as a skimmer well. Together, equations 3.3 and 3.10 then give

$$\frac{db_o}{dt} = -A_s (b_o - \xi) b_o^{\,2} \tag{3.18}$$

This equation may be integrated to give

$$\frac{1}{\xi b_o(t)} - \frac{1}{\xi b_o(0)} + \frac{1}{\xi^2} \ln\left[\frac{(b_o(t) - \xi) b_o(0)}{(b_o(0) - \xi) b_o(t)}\right] = -A_s t \tag{3.19}$$

In equations 3.18 and 3.19,

$$A_s = \frac{(\rho_w - \rho_o) \rho_o \mu_w K_w \eta}{R_c^{\,2} (\beta - \gamma) \rho_w^{\,2} \mu_o \ln(R/r_w)} = \frac{(1 - \rho_r) \rho_r K_w \eta}{R_c^{\,2} (\beta - \gamma) \mu_r \ln(R/r_w)} \tag{3.20}$$

When $\xi = 0$, equation 3.18 becomes

$$\frac{db_o}{dt} = -A_s\, b_o^{\,3} \tag{3.21}$$

The integral of equation 3.21 is

$$b_o(t) = b_o(0)\sqrt{\frac{1}{1 + 2\,A_s\, b_o(0)^2\, t}} \tag{3.22}$$

Equations 3.19 and 3.22 with 3.20 provide the performance equations for a skimmer well.

3.1.5 Recovery Volume

The performance equations provide the monitoring well LNAPL thickness as a function of time. In the case of equation 3.19, this is an implicit function and must be handled differently than the others. Once $b_o(t)$ is known, the volume recovered during a time increment $\Delta t = t_2 - t_1$ may be calculated from

$$\Delta V_o(\Delta t) = \pi R_c^{\,2}(\beta - \gamma)\left(b_o(t_1) - b_o(t_2)\right) \tag{3.23}$$

Furthermore, the LNAPL discharge may be calculated using equations 3.1, 3.2 or 3.3.

3.2 LNAPL Recovery Using Trenches

The same modeling framework may also be used to represent a simple trench recovery system, such as shown in Figure 1.3. The rate of LNAPL recovery can be enhanced through production of water from the trench. Otherwise, the natural groundwater gradient J_w is responsible for the movement of LNAPL into the trench where it is removed by skimmer wells or other technology.

The rate of LNAPL flow into the trench depends on both the hydraulic gradient within the LNAPL layer and the effective layer relative permeability. The LNAPL discharge may be calculated from

$$Q_o(t) = W_T\, b_o(t)\bar{k}_{\mathrm{ro}}(b_o)K_o\, J_o \tag{3.24}$$

In equation 3.24, the trench discharge varies with time because the effective LNAPL layer thickness decreased in with time, and because the LNAPL layer relative permeability is a function of the lens thickness. The lens gradient is the same as the

natural groundwater hydraulic gradient (i.e., $J_o = J_w$) unless there is groundwater production from the trench. In this latter case, it is assumed through superposition that groundwater production creates an inward gradient on each side of the lens, and the resulting LNAPL layer gradient may be calculated from

$$J_o = J_w + \frac{Q_w}{2 K_w W_T b_w} \tag{3.25}$$

In equation 3.25 b_w is the effective groundwater capture depth of the trench.

The continuity equation for the LNAPL lens may be written following equation 3.11 in the form

$$\frac{db_o}{dt} = -\left(\frac{\eta K_o J_o}{L_T (\beta - \gamma)} \right) b_o \left(b_o - \xi \right) \tag{3.26}$$

Equation 3.26 has the same form as equation 3.12 with solution given by equations 3.14 and 3.15. These provide the performance equations for the trench recovery system. The factor A_k is specified by the term within brackets in equation 3.26. More explicitly, this factor may be written

$$A_T = \frac{\rho_o \mu_w \eta K_w}{\rho_w \mu_o L_T (\beta - \gamma)} \left(J_w + \frac{Q_w}{2 K_w W_T b_w} \right) \tag{3.27}$$

Note that for both the trench and the skimmer well, the aquifer hydraulic conductivity appears explicitly in the performance equations.

If the trench bisects an LNAPL lens, then the recovery model may be applied separately to each section of the lens. This is only feasible if water is also produced from the trench to create an inward gradient on each side. For the section on the downgradient side of the trench, the natural gradient J_w should be specified as a negative number.

SECTION 4 – MODEL IMPLEMENTATION AND APPLICATIONS

The models described in Section 3 have been implemented through two separate and standalone spreadsheets: *LNAPL (vG-B).xls and LNAPL (vG-M).xls.* As the naming attempts to imply, these two models are for homogeneous soil with the van Genuchten soil characteristic model, and with application of the Burdine and Mualem models for calculation of the relative permeability. This section describes the spreadsheet models, an example application, features of model implementation, and case study applications.

4.1 Spreadsheet Models

Each of the spreadsheet models has one worksheet for entry of basic data (Data Entry). A second worksheet (Layer Calcs) is used in calculation of LNAPL-layer specific volume and relative permeability parameters (χ_i, β_i, ξ_i, η_i; i = 1,2,3) from equations 2.25 and 2.30, where the index is associated with each of the three linear segments. To facilitate calculation of these parameters, a series of 26 data values (D_o and k_{ro} as a function of b_o) are calculated using the model equations presented in Section 2. Identification of the three linear segments requires specification of four sets of values $(b_o, D_o, k_{ro})_j$, j = 0, 1, 2, 3. The sets corresponding to j-values 0 and 3 are specified by the model: $(0, 0, 0)_0$ and $(b_{omax}, D_o(b_{omax}), k_{ro}(b_{omax}))_3$, where b_{omax} is the maximum LNAPL monitoring well thickness that is specified on the Data Entry worksheet. The other two sets are selected from the series of 26 data values that have been calculated (as shown below). The third worksheet (Distribution Charts) allows viewing of the LNAPL, reduced-LNAPL (with residual saturation values set to zero), and water saturation profiles, and the LNAPL relative permeability profile for selected values of the monitoring well LNAPL thickness b_o. The fourth worksheet (Well) is for calculation of the LNAPL recovery. Required variables for water or air-enhanced systems, or for skimmer wells are entered, and the time history of the LNAPL thickness, volume recovery, and recovery rate are calculated and shown graphically. The fifth worksheet (Trench) calculates LNAPL recovery using a trench. A description of model application follows.

4.2 Example Model Application

This subsection outlines the model application for the sand soil with characteristic curve shown in Figure 2.1. Each of the model worksheets is described, and model parameters and application are discussed.

4.2.1 Data Entry Worksheet

This example shows the model application for the soil characteristic curve shown in Figure 2.1, leading to Figure 2.2 for a LNAPL layer in a sand soil. Figure 4.1 shows the basic Data Entry worksheet. The maximum LNAPL monitoring-well thickness is specified. The LNAPL specific storage and relative permeability models are fit for thickness values from zero to this maximum thickness. This is also the starting thickness for estimation of recovery time and LNAPL recovery volumes and rates. The soil characteristic variables include the irreducible water content and the residual LNAPL saturation for the saturated and vadose zones. Fluid characteristics include the LNAPL density and surface/interfacial tension values. Appropriate units are shown. Calculated parameters include the maximum free-product elevation (using equation 2.23) and the Brooks and Corey soil characteristic parameters that correspond to the selected van Genuchten variables.

Maximum Monitoring Well LNAPL Thickness [feet]	
b_o =	3.000

Soil Characteristic		
n =	0.400	porosity
N =	4.000	van Genuchten "N"
α =	2.000	van Genuchten "α" [ft^{-1}]
S_{wr} =	0.150	irreducible water saturation
S_{orv} =	0.050	residual LNAPL saturation (saturated)
S_{ors} =	0.150	residual LNAPL saturation (vadose)

Fluid Characteristics:		
ρ_o =	0.750	LNAPL density [gm/cc]
σ_{aw} =	65.000	air/water surface tension [dyne/cm]
σ_{ao} =	25.000	air/LNAPL surface tension [dyne/cm]
σ_{ow} =	25.000	LNAPL/water surface tension [dyne/cm]

Calculated Parameters		
M =	0.750	van Genuchten "M"
α_{ao} =	3.900	air/LNAPL "α" [ft^{-1}]
α_{ow} =	1.300	LNAPL/water "α" [ft^{-1}]
z_{ao} =	0.750	elevation of air-LNAPL interface [ft]
z_{ow} =	-2.250	elevation of LNAPL-water interface [ft]
z_{max} =	2.180	maximum free-product elevation [ft]
λ =	1.809	pore-size distribution index
Ψ_b =	0.359	B-C displacement pressure head [ft]

Press Ctrl-Shift+S to calculate sheet

Figure 4.1. Data Entry worksheet shows data leading to Figure 2.2. Only the data on the left side are entered. The parameters on the right are computed from entered data.

4.2.2 Layer Calcs Worksheet

Once the basic data are entered (and computed), the second worksheet calculates values of D_o and k_{ro} for twenty-six equally spaced b_o-values within the range from 0 to the maximum value specified at the top of Figure 4.1. These values are plotted, as shown in Figure 4.2, with the triangles corresponding to the LNAPL specific volume and the diamonds the relative permeability values. The integrals expressed by equations 2.24 and 2.29 are evaluated using Simpson's rule, and the parameters Eps-Do and Eps-kro give the iteration convergence tolerance for each integral approximation. The smaller the value, the more accurate the calculation of $D_o(b_o)$ and $k_{ro}(b_o)$, and the longer the computation time. Strategically, it is probably best to start with a larger value (say 0.001), look at the resulting data curve that should be smooth and well behaved, and then decrease the value as necessary.

Data for curve-fitting segments				Press Ctrl-Shift+S to calculate sheet				
b_o	D_o	k_{ro}	χ	β	ξ	η		
0.000	0.000	0.000						
0.240	0.025	0.000	0.0000	0.105203	0.0000	0.000006		
1.080	0.219	0.127	0.1305	0.230559	0.2400	0.150923	0.0001	Eps-Do
3.000	0.876	0.455	0.4401	0.342086	0.3374	0.170711	0.00001	Eps-kro

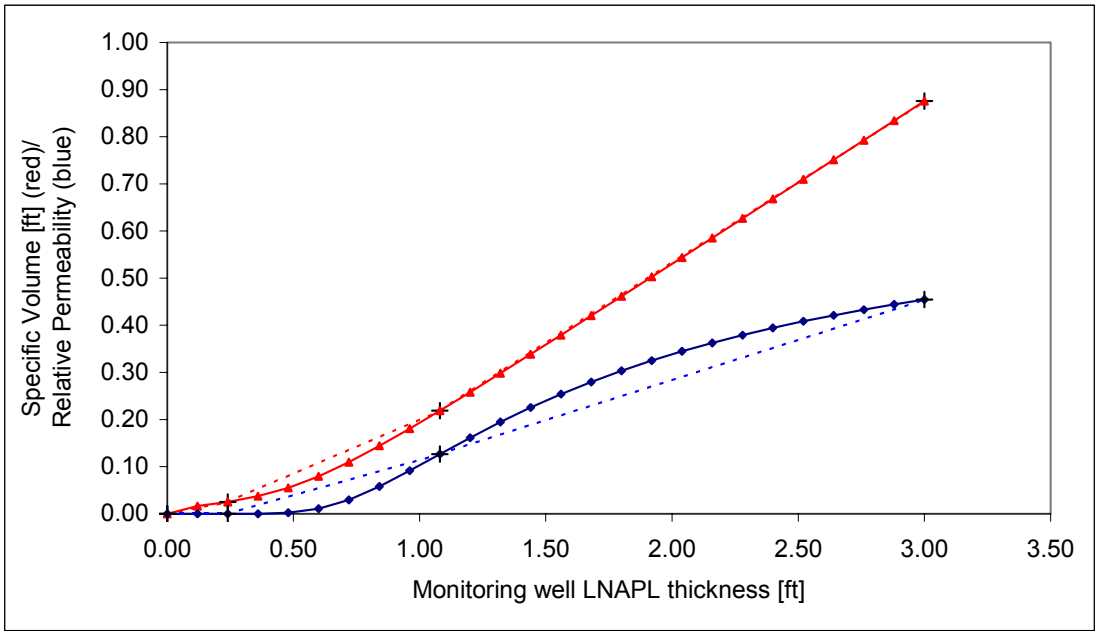

Figure 4.2. Parameter fitting worksheet Layer Calcs before selection of curve-fitting values $(b_o,D_o,k_{ro})_1$ *and* $(b_o,D_o,k_{ro})_2$.

On the Layer Calcs spreadsheet page, the table of 26 calculated values of b_o, D_o and k_{ro} are listed below the figure that is shown in Figure 4.2, in rows 40-65 and columns B-D of the spreadsheet. These values correspond to 26 equally-space values of b_o within the range 0-b_{omax}. Thus for this example, the spacing is $\Delta b_o = b_{omax}/25 = 3.0/25 = 0.12$ feet, and the $(b_o)_j$ series has values (0, 0.12, 0.24, 0.36, …). The dashed linear segments in Figure 4.2 correspond to selection of the 3rd and 10th values from this series (which can be seen by counting the number of diamonds or triangles on the data curves, starting with the first point at the origin). The fitting of the dashed curve to the data curve is especially poor for the relative permeability function (marked by diamonds).

Figure 4.3 shows the working table for fitting of the linear-segment models D_o-b_o and k_{ro}-b_o. The 6 circled values are read from the table of calculated values in columns B to D and rows 40-65. The set (b_o, D_o, k_{ro}) = (0.240, 0.025, 0.000) is read from the 3rd row of this table (row 42) and represents the cells (B42, C42, D42). Likewise, the

second set is from row 59 (10^{th} set of values from the table), and represents cells (B49, C49, D49). The first set of values is automatically set to (0, 0, 0) while the fourth set is read from the last row of the table of calculated values: (B65, C65, D65). The linear segment parameters (α,β,ξ,η) are calculated from the four sets (b_o, D_o, k_{ro}). For example, $\beta = \Delta D_o/\Delta b_o$, so that β_1 = (0.025[2] – 0.000)/(0.240 – 0.000) = 0.105, etc.

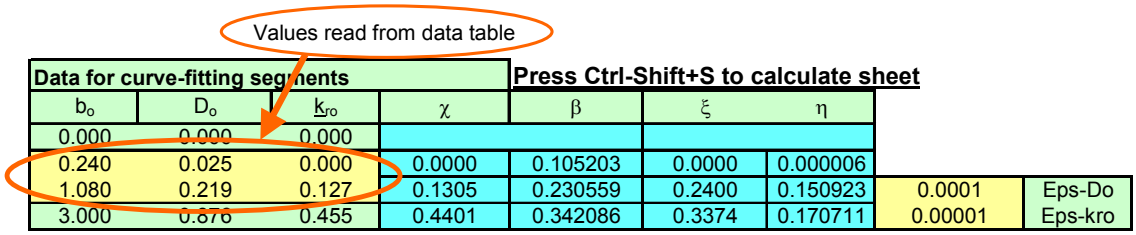

Figure 4.3. Working table for fitting linear-segment models

To improve the linear-segment fit, a different row from the data table of calculated values needs to be selected. Inspection of Figure 4.2 suggests that the 6^{th} and 16^{th} sets might be better (rows 45 and 55 from the spreadsheet). Click on the cell containing $(b_o)_2$ = 0.240 (this is cell B5 of the spreadsheet). Its contents read "=B42" (do not include the quotation marks!). Change this to read "=B45", and do similarly for the other five values. The contents of the six circled cells in Figure 4.3 should read (=B45, =C45, =D45) and (=B55, =C55, =D55). Press "Ctrl+Shift+S" to recalculate the spreadsheet page. The results shown in Figure 4.4 should appear.

Data for curve-fitting segments				Press Ctrl-Shift+S to calculate sheet				
b_o	D_o	k_{ro}	χ	β	ξ	η		
0.000	0.000	0.000						
0.600	0.080	0.011	0.0000	0.132704	0.0000	0.017535		
1.800	0.461	0.303	0.3497	0.318167	0.5569	0.244062	0.0001	Eps-Do
3.000	0.876	0.455	0.4635	0.345251	-0.6087	0.125956	0.00001	Eps-kro

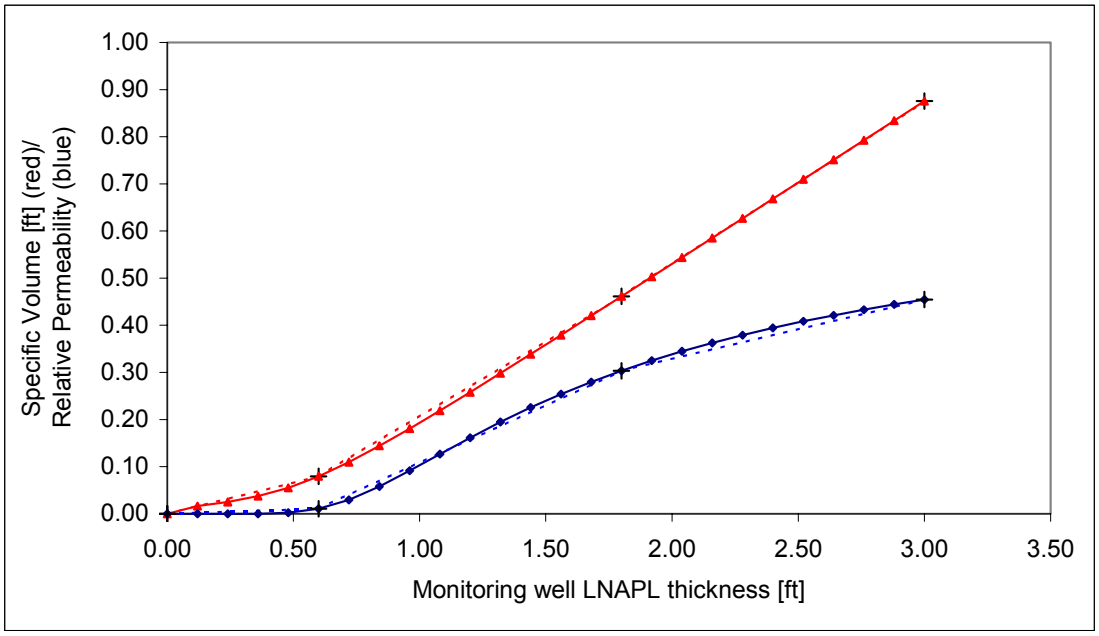

Figure 4.4. Fitted version of linear segment models for D_o-b_o and k_{ro}-b_o

Discussion: The procedure described above involves visually selecting the best-fitting points and manually changing the data cells that are read into the graph and used in calculations. One might simplify this procedure by using available tools such as the Excel "SOLVE" function. However, experience suggests that the required constraints vary from problem to problem. In addition, the only goal is to capture the general shape of the two functions D_o-b_o and k_{ro}-b_o. Because of the overall simplicity of the model formulation, any attempts to improve on accuracy at this point are probably not warranted.

4.2.3 Distribution Charts Worksheet

With the basic data entered in the Data Entry worksheet, the distribution of saturation and relative permeability may be viewed in the third worksheet (Distribution Charts), as shown in Figure 4.5 (see Figures 2.5, 2.6 and 2.7 for a description of the contents of this chart). This worksheet is linked only with the Data Entry worksheet, and thus the Data Entry worksheet must be calculated before the distribution charts can be evaluated. The "Monitoring Well LNAPL Thickness b_o" value may be changed and the sheet recalculated to see how the saturation and relative permeability curves vary with LNAPL-layer thickness. The D_o and k_{ro} values that are shown correspond to the calculated values from equations 2.24 and 2.29 for the selected b_o value.

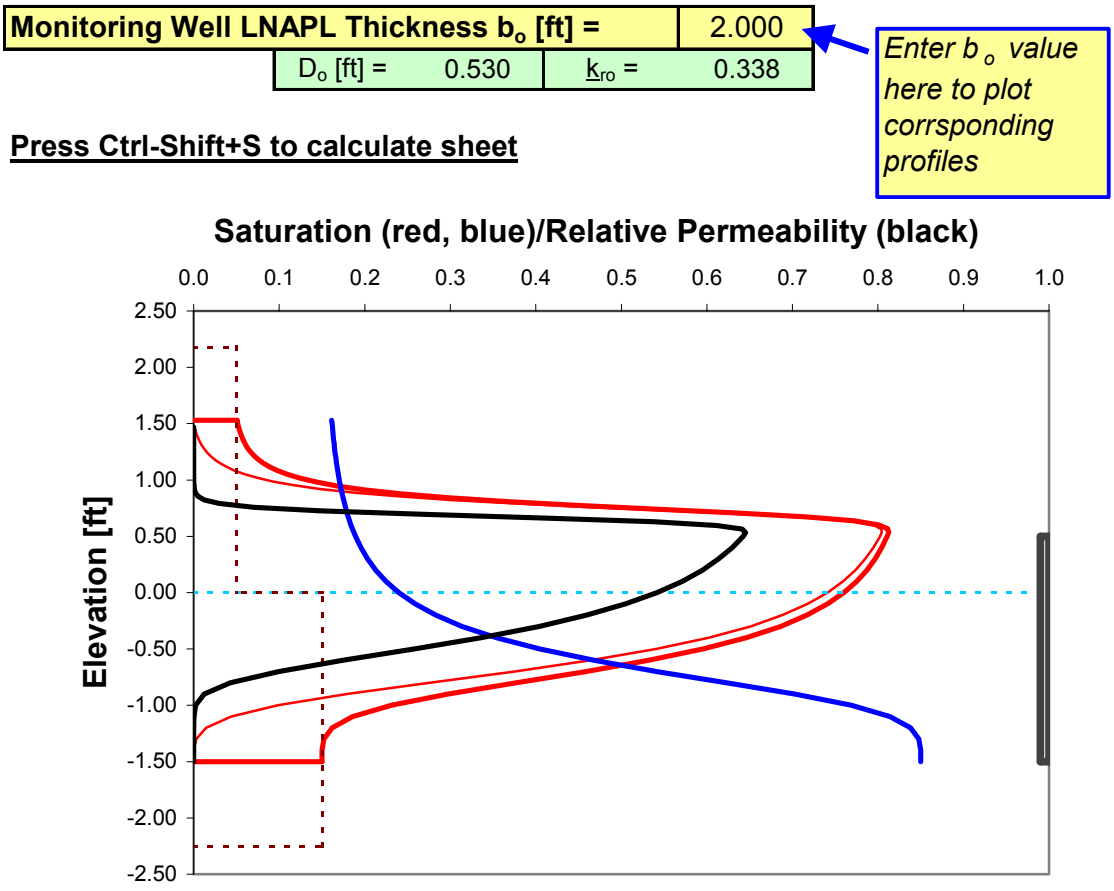

Figure 4.5. Saturation and relative permeability distribution

4.2.4 **Well Worksheet**

Free-product recovery system analysis may be performed using worksheet 4 for wells and worksheet 5 for a trench recovery system. First consider a recovery system using wells and worksheet 4 (Well). The basic design variables required in this worksheet are the recovery time, the recovery system (well) radius of capture, which is a basic design variable as described in Charbeneau et al. (1999), and the LNAPL dynamic viscosity. Separate sets of data are required for estimation of system response and for specification of water enhanced and vacuum enhanced system performance. The formation hydraulic conductivity and recovery well radius are specified. These are used explicitly in calculation of LNAPL recovery using skimmer wells. For water-enhanced and vacuum-enhanced systems, these data are used to calculate response of the subsurface system to water/air production. If both the water discharge and the wellhead suction pressure are set to zero, then a skimmer well is assumed.

For a water-enhanced LNAPL recovery system the model requires the water production rate and the screened interval of the aquifer. These are used directly in calculation of the LNAPL recovery rate (see equation 3.1). To estimate the response of the subsurface system to water production, the well radius of influence is also required. This estimated value will not affect the predicted LNAPL recovery rates, but it is used to calculate the drawdown at the well and the average drawdown within the radius of capture. The drawdown at the well is calculated using the Thiem equation.

For a vacuum-enhanced LNAPL recovery system the model requires specification of the wellhead suction pressure, the screened section of the vadose zone, and an estimate of the air-phase relative permeability within the vadose zone. The wellhead suction pressure is used to calculate the resulting air-phase production rate, and these variables are used to calculate the LNAPL recovery rate using equation 3.2.

Figure 4.6 shows the parameters and output for the worksheet data of Figure 4.1 for a water-enhanced system producing 5 gallons per minute (gpm). The first graph shows the LNAPL monitoring well thickness as a function of time. Two points are marked (in red) on the LNAPL thickness chart. These points correspond to transition

between segments of the linear-segment models for D_o-b_o and k_{ro}-b_o. The parameters for segment 3 are used for the first 0.23 years, and segment 2 for the time period between 0.23 years and 2.8 years. If the time epoch for reaching either of the points does not occur within the recovery range $t_{recovery}$, then the points are not shown. The second graph shows the recovery volume (the dashed line is the total LNAPL volume within the radius of capture, based on the initial LNAPL monitoring well thickness; see equation 3.4). The third graph shows the recovery rate as a function of time. The LNAPL recovery rate drops from a maximum value of nearly 250 gallons per day (gpd) to approximately 1 gpd after 3 years. The chart shows clearly that most of the recovery occurs during the first year. During the 3rd year, the predicted LNAPL recovery is approximately 500 gallons and requires more than 2.6-million gallons of water production.

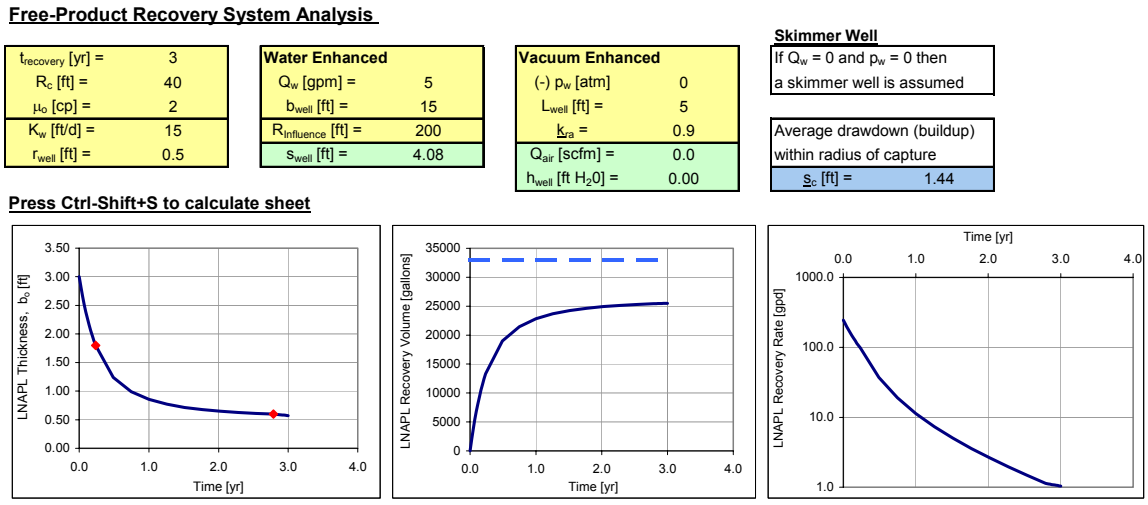

Figure 4.6. Free-product recovery worksheet showing water-enhanced recovery performance

For water-enhanced or vacuum-enhanced recovery systems, the model calculates the average drawdown (or buildup) of the water table within the region between the recovery well and the radius of capture. This is calculated as follows. Consistent with the Thiem equation, the drawdown at any radius r is given by

$$s(r) = s_{\text{well}} \ln\left(\frac{R_I}{r}\right) \Big/ \ln\left(\frac{R_I}{r_w}\right) \qquad (4.1)$$

In equation 4.1, R_I is the radius of influence of the well and s_{well} is the drawdown at the well. The average drawdown within the annulus between the well radius and the radius of capture is calculated from

$$\bar{s}_c = \frac{1}{\pi\left(R_c^{\,2} - r_w^{\,2}\right)} \int_{r_w}^{R_c} 2\pi r\, s(r)\, dr \qquad (4.2)$$

Substituting equation 4.1 into 4.2 and evaluating the integral one finds

$$\bar{s}_c = s_{well}\left[\frac{R_c^{\,2}\ln\left(R_I^{\,2}/R_c^{\,2}\right) - r_w^{\,2}\ln\left(R_I^{\,2}/r_w^{\,2}\right)}{\left(R_c^{\,2} - r_w^{\,2}\right)\ln\left(R_I^{\,2}/r_w^{\,2}\right)} + \frac{1}{\ln\left(R_I^{\,2}/r_w^{\,2}\right)}\right] \qquad (4.3)$$

The same equation is used for the water table buildup with the vacuum-enhanced system, with h_{well} replacing s_{well} and it is assumed that $R_I = R_c$ for the vacuum-enhanced system. Use of the average drawdown/buildup is discussed in Section 4.3.

For comparison with the water-enhanced system, Figure 4.7 shows the performance of the same system using skimmer wells with a radius of capture of 15 feet and for a recovery period of 5 years. The potential recovery is much less than shown in Figure 4.5 because the radius of capture is smaller. During the recovery period the LNAPL recovery rate decreases from about 40 gpd to just over 0.1 gpd at 5 years. As suggested by Figure 4.4, reduction of LNAPL thickness below 0.6 feet using liquid recovery will be very difficult because the LNAPL relative permeability has been reduced to very low values.

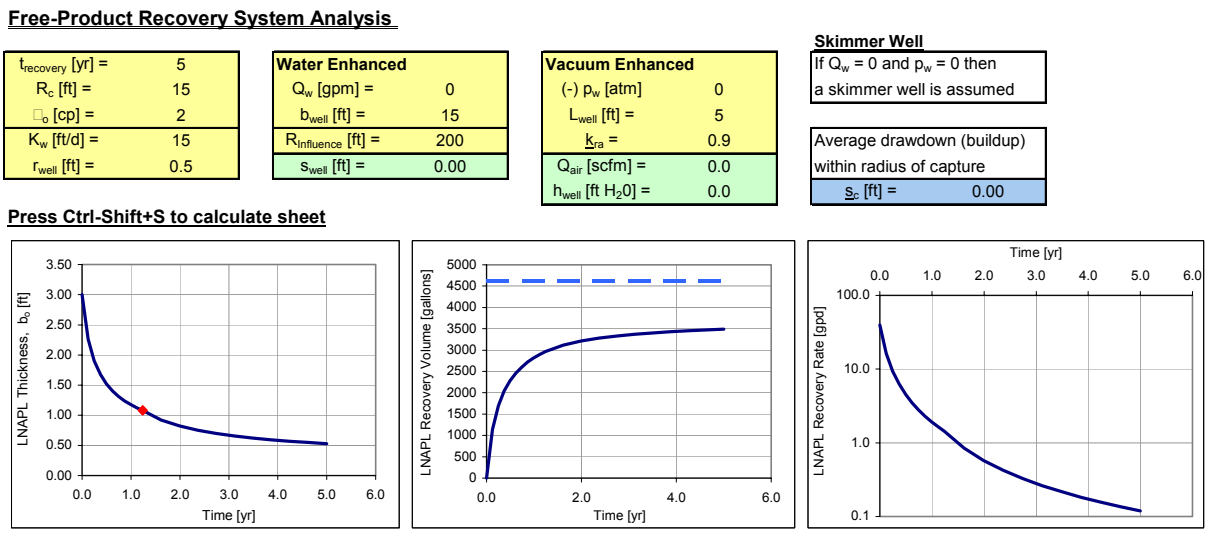

Figure 4.7. Free-product recovery worksheet showing skimmer well recovery performance

4.2.5 Trench Worksheet

Figure 4.8 shows results from worksheet 5 (Trench) for a trench recovery system. The LNAPL lens is assumed to be 75 feet wide by 100 feet long in the direction of natural groundwater flow. The natural groundwater gradient is 0.005. The trench has a capture depth for groundwater of 5 feet. This value is used only in calculating the additional gradient towards the trench caused by recovery of groundwater in addition to LNAPL. It does not enter into calculation of LNAPL recovery rates. A groundwater recovery rate of 2 gpm is assumed, which increases the hydraulic gradient towards the lens by a small amount, which in turn, increases the LNAPL recovery rate by a small amount. Comparing Figures 4.5, 4.6 and 4.7, the volume of free-product within the capture zone of the system increases, as does the area size of the capture zone. Considering trenches versus wells, the volume ratio is $(L_T W_T)/(\pi R_c^2)$. Most of the LNAPL recovery occurs within the initial 2-year period. After about 6 years, the recovery rate has decreased to less than 1 gpd.

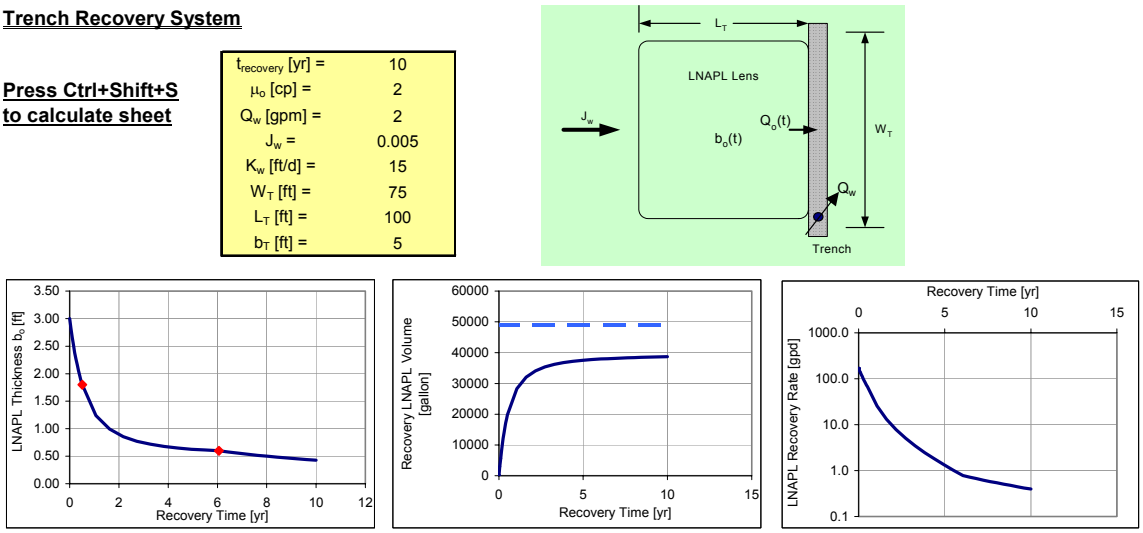

Figure 4.8. Free-product recovery system performance for a trench system

All of the examples presented in this subsection have used the Burdine version of the spreadsheet model [*LNAPL (vG-B).xls*]. All worksheets are the same for the Mualem version of the model, whose use is discussed in Section 4.4.

4.3 LNAPL and Water Table Fluctuations

The formation LNAPL saturation distribution and monitoring well LNAPL thickness will vary with water table fluctuations. If changes in water table elevation are sufficiently slow, the condition of vertical equilibrium will not be compromised to a significant extent, and the discussion presented in Section 2.1 describing the LNAPL saturation distribution remain valid. It is of interest to investigate how D_o and b_o vary with changes in elevation of the water table. To proceed in this investigation, consider an LNAPL layer that has been spread (smeared) across a thickness from a lower elevation z_{sz} in the saturated zone beneath the free-product layer to an upper elevation z_{vz} in the vadose zone above the free product layer. Except within the free-product layer, LNAPL is present at residual saturations in the vadose zone and saturated zone. Using the notation from Section 2.1, the total LNAPL thickness is given by

$$L_{\mathrm{LNAPL}}(0) = n S_{\mathrm{ors}}\left(z_{\mathrm{ow}} - z_{\mathrm{sz}}\right) + D_o + n S_{\mathrm{orv}}\left(z_{vz} - z_{\max}\right) \qquad (4.4)$$

In equation 4.4, free product exists between elevations z_{ow} and z_{max}, the latter being found using equation 2.23, and the specific free-product volume D_o is given by equation 2.24. If the elevation of the water table changes by an amount Δz_{wt} due to groundwater pumping, seasonal hydrologic budget, or other cause, without affecting the amount of LNAPL present, then $L_{LNAPL}(\Delta z_{wt}) = L_{LNAPL}(0)$. Under the new conditions, which are designated by addition of a prime, equation 4.4 becomes

$$L_{\mathrm{LNAPL}}\left(\Delta z_{\mathrm{wt}}\right) = n\,S_{\mathrm{ors}}\left(z_{\mathrm{ow}}{}' - \left(z_{\mathrm{sz}} - \Delta z_{\mathrm{wt}}\right)\right) + D_o{}' + n\,S_{\mathrm{orv}}\left(\left(z_{\mathrm{vz}} - \Delta z_{\mathrm{wt}}\right) - z_{\max}{}'\right) \quad (4.5)$$

Setting the expressions in equations 4.4 and 4.5 equal and simplifying gives

$$nS_{\mathrm{ors}}z_{\mathrm{ow}} + D_o - nS_{\mathrm{orv}}z_{\max} = n\,S_{\mathrm{ors}}z_{\mathrm{ow}}{}' + D_o{}' - n\,S_{\mathrm{orv}}z_{\max}{}' + n\left(S_{\mathrm{ors}} - S_{\mathrm{orv}}\right)\Delta z_{\mathrm{wt}} \quad (4.6)$$

The initial monitoring well thickness may be used with the spreadsheet to evaluate the right side of equation 4.6. Then if Δz_{wt} is known, the spreadsheets may be used iteratively to evaluate the new monitoring well LNAPL thickness, b_o', and free-product thickness, D_o'.

With the piecewise linear model equations, the calculation is made much simpler. Equations 2.19 and 2.20 give $z_{ow} = -\,\square_r\, b_o$, $z_{ao} = (1 - \rho_r)\, b_o$, and $b_o = z_{ao} - z_{ow}$. Using these along with equation 2.25, equation 4.6 may be written

$$\left(\beta - \gamma\right) b_o - \beta\chi = \left(\beta' - \gamma\right) b_o' - \beta'\chi' + n\left(S_{\mathrm{ors}} - S_{\mathrm{orv}}\right)\Delta z_{\mathrm{wt}} \quad (4.7)$$

Equation 4.7 may be solved directly for the new monitoring well thickness giving

$$b_o' = \frac{\left(\beta - \gamma\right) b_o - \beta\chi + \beta'\chi' - n\left(S_{\mathrm{ors}} - S_{\mathrm{orv}}\right)\Delta z_{\mathrm{wt}}}{\left(\beta' - \gamma\right)} \quad (4.8)$$

An example will highlight the significance of these results. Consider the initial condition shown in Figure 2.2 with a monitoring-well LNAPL thickness of 2 feet. The spreadsheet model gives z_{ow} = - 1.5 feet, z_{max} = 1.530 feet, and D_o = 0.530 feet, so the right side of equation 4.6 has the value 0.4094 feet. According to Figure 4.6, a water production rate of 5 gpm results in an average drawdown of 1.44 feet within the 40-foot radius of capture. If the water table is lowered by 1.44 feet (Δz_{wt} = -1.44 ft), then $n(S_{ors}$-$S_{orv})\Delta z_{wt}$ = -0.0576 feet. Thus the remaining terms on the right side (primed terms) have a combined value of 0.4670 feet. Through trial and error, equation 4.6 is solved to find

b'_o = 2.20 feet, z_{ow} = -1.650 feet, z_{max} = 1.670 feet, and D_o = 0.599 feet. The initial LNAPL saturation distribution and that predicted after the 1.44-feet decrease in water table elevation are shown in Figure 4.1.

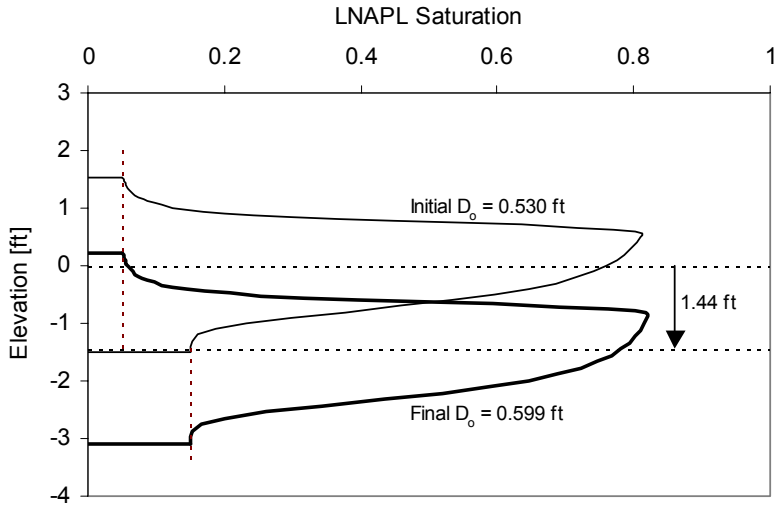

Figure 4.9. LNAPL saturation distribution before and after a 1.44-feet decrease in the water table elevation

Equation 4.8 provides a much simpler solution for finding the change in free-product volume associated with a change in water table elevation. Figure 4.4 shows the data table and fitted curves for the LNAPL-layer specific volume and relative permeability. For an initial monitoring well thickness of 2 feet, the α and β values for the third segment are used (α = 0.4635 and β = 0.345251). The new thickness is greater than 2 feet so the same values are used for α' and β' (the appropriate parameter values for the segment of the D_o-b_o model curve are used). The parameter γ equals 0.0500 (this parameter value is given on both the Well and Trench worksheets, immediately below the charts). Using these values in equation 4.8 gives b'_o = 2.195 feet and D'_o = 0.345251 (2.195 – 0.4635) = 0.5978 feet. These results are essentially the same as found using the first method.

To account for the change in water table elevation due to groundwater pumping, the LNAPL recovery would be calculated with a starting value b_o = 2.2 feet rather than

b_o = 2 feet. That is, the value b_o = 2.2 feet would be entered for the Maximum Monitoring Well LNAPL Thickness on the Data Entry worksheet shown in Figure 4.1.

4.4 Application of the Model to Fine-Grain Soils

Analysis of LNAPL recovery in fine-grain soils is important for a number of reasons. The presence of fine-grain soils near the ground surface is common. The effects of secondary porosity often dominate the hydraulics and transport characteristics of these soils. Furthermore, strong vertical hydraulic gradients are often present. These latter two characteristics are contrary to the assumptions on which the LNAPL recovery model is based (homogeneous soils and vertical equilibrium), and these characteristics may result in "unusual" distributions of LNAPL. For these reasons, discussion of fine-grain soils deserves separate attention.

Primary porosity refers to the original porosity of the porous medium upon deposition. Secondary porosity refers to that portion of the total porosity resulting from diagenetic processes such as dissolution, stress fractures, desiccation cracks, animal burrows, root holes, or other causes. In fine-grain soil the magnitude of secondary porosity (usually called macropores) is usually much smaller than primary porosity, though its existence may dominate the hydraulic characteristics of the porous medium. The length-scale (pore size) associated with the primary porosity is much smaller than that of the secondary porosity. Thus, according to the Laplace equation 2.2, LNAPL can enter the secondary porosity (macropores) at a much smaller capillary pressure then would be required for entrance into the primary porosity (the fine-grain porous matrix). If the secondary porosity forms a continuous porous network, then LNAPL can migrate through this secondary porosity domain, independent of the existence of the primary porosity domain. This can result in unusual distributions and migration patterns for LNAPL.

The presence of strong vertical gradients through fine-grain soil layers is expected near regions of groundwater recharge, especially under conditions where there is an underlying permeable layer. The downward gravitational hydraulic gradient within the vadose zone is 1. When infiltration reaches the water table, it will move both

vertically and horizontally following the hydraulic path of least resistance. With an underlying permeable layer, this path is generally downward, and movement of recharge water through the fine-grain layer (with low permeability) requires a strong downward gradient. Downward vertical gradients may be one to three orders of magnitude larger than horizontal gradients.

4.4.1 Conceptual Model for LNAPL Distribution in Fine-Grain Soil

First consider the potential depth of LNAPL penetration below the water table in fine-grain soil. The schematic in Figure 4.10 shows an LNAPL source zone located a distance Z_o above the water table. LNAPL has entered the macropore system and migrated downward to a depth Z below the water table. At point *B* located at this depth Z below the water table, the water and LNAPL pressure are the same (there is negligible capillary pressure within the macropore because of its size). The pressure through the LNAPL may be calculated using hydrostatics, while the water pressure must consider the downward movement of percolating water under a hydraulic gradient J_z. Equating the pressures at point *B* gives the following relationship:

$$Z = \left(\frac{\rho_r}{1 - \rho_r - J_z} \right) Z_o \qquad (4.9)$$

Equation 4.9 shows that in particular, if $J_z > 1 - \rho_r$, then the hydraulic gradient will carry the LNAPL down to the underlying permeable zone where the vertical hydraulic gradient should be dissipated.

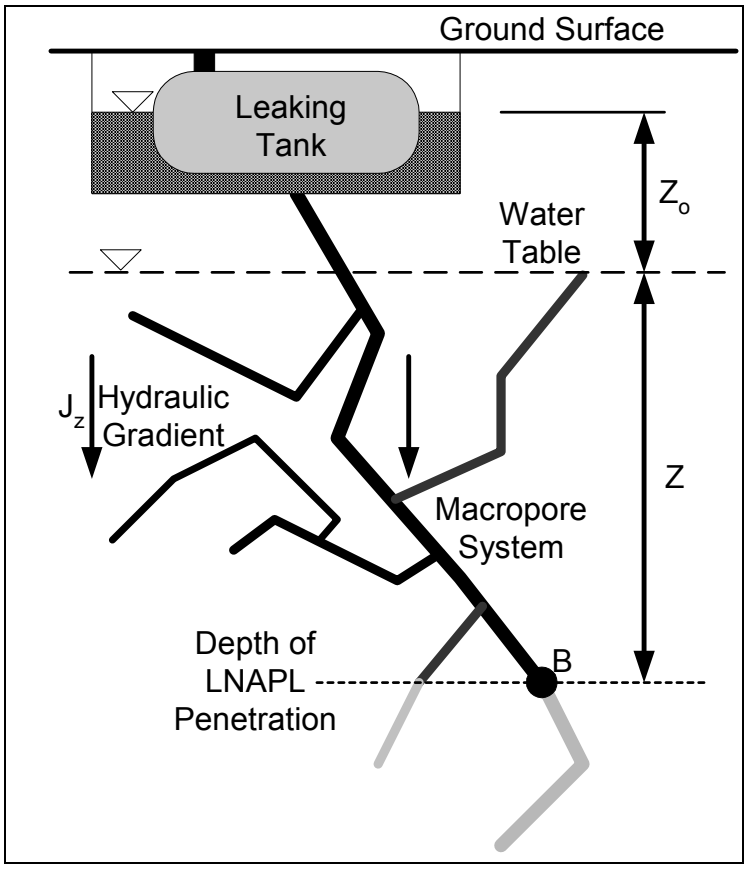

Figure 4.10. Schematic view of LNAPL distribution in macropores

Equation 4.9 suggests that LNAPL can penetrate to considerable depths within macropores of a fine-grain soil. If the macropores are in direct communication with a monitoring well, then the same LNAPL thickness will be observed in the well. However, because LNAPL is confined to the macropores, the overall LNAPL saturation remains very low. This is one of the unusual features of fine-grain soils. One may expect to find large LNAPL thickness in monitoring wells with adjacent soils having very low LNAPL saturation.

4.4.2 Characterization of a Fine-Grain-Soil Site

Data was provided for a site located in the Midwestern United States (Adamski et al., 2003). At this location, the subsurface consists of about 27 feet of homogeneous

fine-grain soil overlying a thin, discontinuous layer of weathered bedrock and competent, relatively impermeable shale/sandstone bedrock. The depth to groundwater is generally 7 to 10 feet below-ground-surface (bgs). The downward vertical gradient through the fine-grain soil ranges from 0.10 to 0.30, while the horizontal gradient is 0.08. LNAPL has been observed in macropores and permeable zones as deep as 17 feet below the water table. LNAPL accumulations in excess of 15 feet have been measured in observation wells.

Water retention data were obtained in the laboratory for a fine-grain soil boring from the site. The van Genuchten model parameters N, α, and S_{wr} were fit to this data, with the soil characteristics curve shown in Figure 4.11. The resulting parameters are N = 1.46, α = 0.17 ft^{-1}, and S_{wr} = 0.69. The saturated water content (porosity) is n = 0.433. Very large suction pressures are required to displace water from the fine-grain soil.

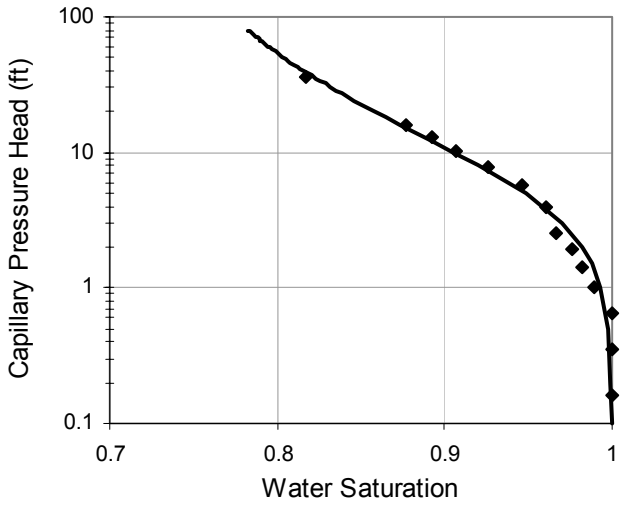

Figure 4.11. Fine-grain soil characteristic curve showing measured data with fitted van Genuchten model (N = 1.46, □ = 0.17 ft^{-1}, and S_{wr} = 0.69)

The LNAPL at this site is a non-volatile weathered diesel. Separate measurements were made of interfacial tension values (σ_{aw} = 66 dyne/cm, σ_{ow} = 20 dyne/cm, σ_{ao} = 31 dyne/cm), LNAPL density (ρ_o = 0.91 g/cm^3), and LNAPL viscosity (μ_o

= 6.3 cp). Analysis of slug test data suggests that the hydraulic conductivity is approximately 0.01 ft/d.

LNAPL saturation values were measured for soil borings located above and below the water table. Eleven analyses were conducted resulting in eight samples without detectable LNAPL, two samples with LNAPL at 0.1% saturation, and one sample with LNAPL at 1.4% saturation (the largest value observed). That most of the samples had no detectable LNAPL might have been expected, because LNAPL is confined to the macropores, and the macropores are spaced through the domain. If macropores are sufficiently sparse, most of the randomly placed soil borings would not contain macropores and associated LNAPL. The field-measured data was input to the model for LNAPL distribution, and the resulting profile is shown in Figure 4.12, where the LNAPL distribution corresponds to a LNAPL monitoring well thickness of b_o = 10 feet. Residual vadose zone and saturated zone LNAPL saturation values are assumed to be zero. This is consistent with the soil borings having no detectable LNAPL. Soil boring data was available in terms of depth bgs. For this figure, it is assumed that the water table is located 7 feet bgs. Perhaps the most significant feature of merit from this figure is that a maximum model-predicted LNAPL saturation of about 2 - 3% is not unreasonable based on the site-specific data, and that this is consistent with monitoring-well LNAPL thickness of about 10 feet.

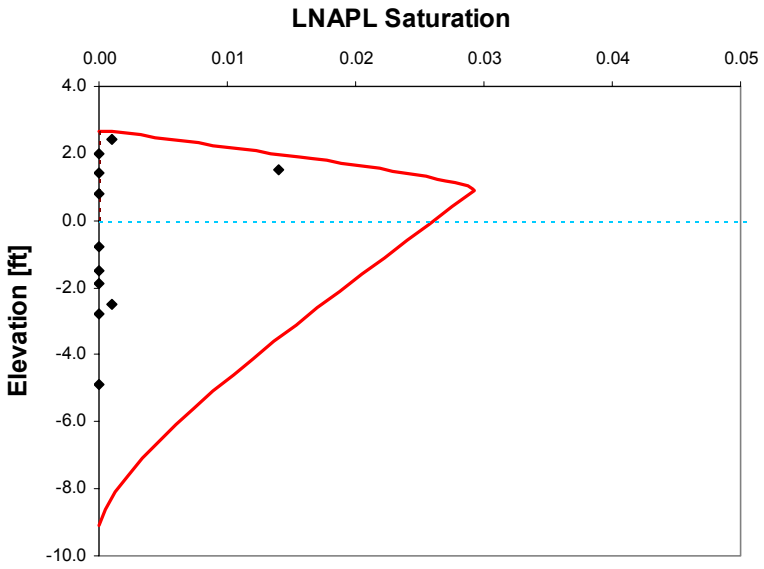

Figure 4.12. LNAPL distribution in fine-grain soil with macropores

The Mualem (1976) model is used to predict the relative permeability distribution. This model was developed using *cut and rejoin* concepts, and Mualem assumed that pore lengths are proportional to pore radii, which results in large pores having "a more important influence than is generally assumed." Use of the Burdine model with these small saturation values will result in essentially zero relative permeability and no LNAPL flow.

A total fluids extraction (TFE) system has been in operation at the site. The recovery system consists of a two-inch well removing air, water and LNAPL, extracted with suction applied via a liquid ring pump. The system applies a vacuum of about 26 inches of mercury to the well (approximately 0.85 atmospheres suction). The screen length of the recovery well is 20 feet. During recovery, the initial airflow rate was 65 standard ft^3/minute (scfm). The initial LNAPL thickness in monitoring wells located near the extraction well varied from 0.55 feet to 15.3 feet.

The spreadsheet model was applied to simulate LNAPL recovery as a vacuum-enhanced system. All measured data were used. An effective radius of capture of 20 feet was assumed, and it is assumed that the average initial LNAPL thickness within this radius is 8 feet. Using this data and a 1-year recovery period, the model predicts recovery of only 40 gallons out of a potential recovery of 390 gallons within the radius of capture. This is compared to the measured recovery of 150 gallons. The reason for the small recovery is the hydraulic conductivity value that is used. Even with a suction pressure of 0.85 atmospheres, the model calculates an air discharge of 0.3 scfm. Increasing the hydraulic conductivity value to 2.55 ft/d (more than a two-order-of-magnitude increase), the predicted air discharge is 65 scfm, which is the same as the initial air discharge from the recovery system. Figure 4.13 shows the resulting measured and predicted LNAPL recovery. The predicted recovery is more than twice as large as the measured recovery after 1 year.

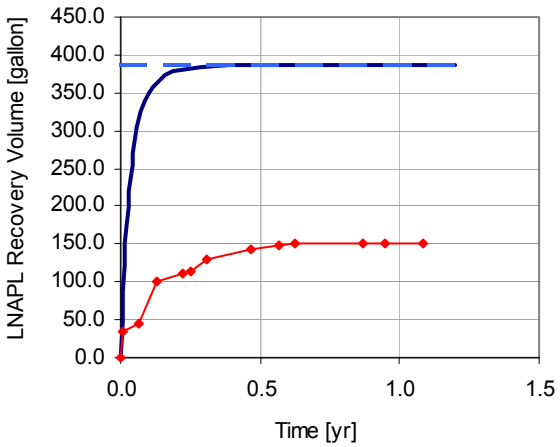

Figure 4.13. Comparison of measured and predicted LNAPL recovery

The objective of this exercise is to show that the model can be applied using measured field data, and that useful results for design and analysis of LNAPL recovery systems can be obtained. Much better fit to the observed recovery data can be achieved with the model by adjusting parameters. Figure 4.14 shows that excellent agreement can be achieved with a radius of recovery R_c = 12.5 feet and a hydraulic conductivity of 1.9 ft/d. However, it is recognized that this excellent fit verifies neither the model nor the parameter values.

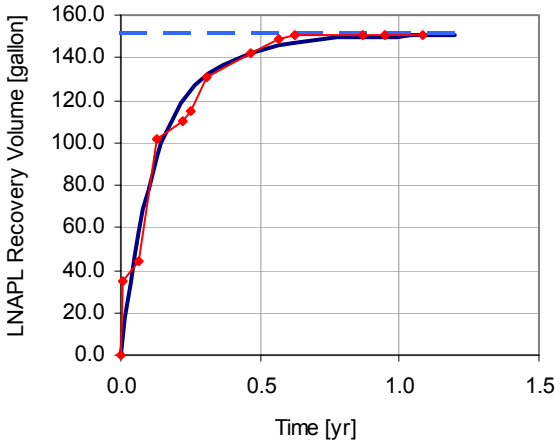

Figure 4.14. Calibrated model with R_c = 12.5 ft and K_w = 0.25 ft/d

4.4.3 Discussion

This is a good point to clarify one aspect of the liquid free-product hydrocarbon recovery model. Looking at Figure 4.13, it appears that an obvious parameter change for obtaining a better fit between the predicted and measured recovery would be to change the LNAPL residual saturation values. However, the effects this will have may not be expected because the capillary pressure head is the primary variable, rather than the LNAPL saturation. Equations 2.8 and 2.10 show that the capillary pressure head at a specified elevation is a function of the elevation of the LNAPL-water and air-LNAPL interfaces in a monitoring well. Based on the capillary pressure head, scaling relations are used to calculate the water (equation 2.13) and total liquid (equation 2.14) saturation values. Changing the residual LNAPL saturation values for the vadose zone and saturated zone will change the total saturation values as well.

The effect of changing the vadose zone and saturated zone residual LNAPL values from zero to S_{orv} = 0.002 and S_{ors} = 0.008 are shown in Figure 4.15. The figure to the left shows the LNAPL saturation and relative permeability distributions. Two curves are shown for the LNAPL saturation. The curve with smaller saturation values has zero-residual values, and is used to calculate the relative permeability distribution. This is the same distribution that was used to predict the recovery shown in Figure 4.13. The second LNAPL saturation curve with larger values is used to estimate specific storage and potential recovery. The right side of Figure 4.15 shows the predicted LNAPL recovery. Compared with Figure 4.14, the potential recovery is seen to increase significantly, while the actual predicted recovery also increases compared with results from the model with zero residual saturation values.

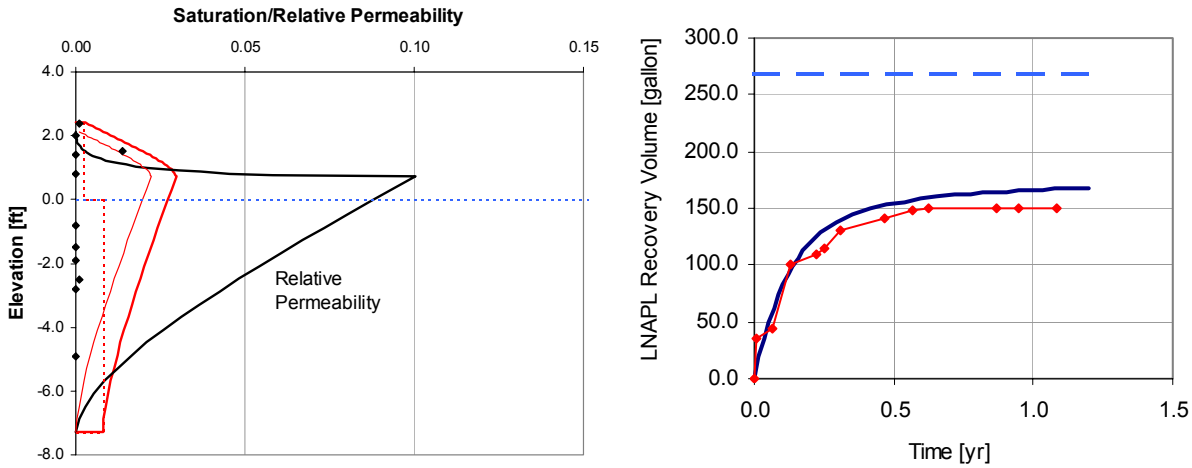

Figure 4.15. LNAPL saturation, relative permeability, and recovery curves for a model simulation with positive LNAPL residual saturation values

4.5 Model Implementation

This liquid free-product recovery model is implemented within an Excel workbook through definition of a number of functions for performing the separate calculations. These functions along with their arguments are listed in Appendix B along with a brief description of the task that each function is performing. [Unlike Fortran or C functions, a function in Visual Basic is meant to only return a single numerical or logical value to the calling spreadsheet cell.]

SECTION 5 – REFERENCES

Adamski, M., Kremesec, V., Kolhatkar, R., Pearson, C., and Rowan, B., LNAPL in Fine-Grained Soils: Conceptualization of Saturation, Distribution, Recovery and Their Modeling, *Ground Water Monitoring & Remediation*, 2003 (Submitted).

Brooks, R.H. and Corey, A.T., Hydraulic Properties of Porous Media, *Hydrol. Pap. 3*, Colo. State Univ., Fort Collins, 1964.

Burdine, N.T., Relative Permeability Calculations from Pore-size Data, *Trans. A.I.M.E. 198*, 71-77, 1953.

Carsell, R.F. and Parish, R.S., Developing Joint Probability Distributions of Soil Water Retention Characteristics, *Water Resources Research, 24*(5), 755-769, 1988.

Charbeneau, R.J., Johns, R.T., Lake, L.W., and McAdams III., M.J., *Free-Product Recovery of Petroleum Hydrocarbon Liquids*, American Petroleum Institute Publication Number 4682, Washington D.C., June 1999.

Charbeneau, R.J., Johns, R.T., Lake, L.W. and McAdams III, M.J., Free-product Recovery of Petroleum Hydrocarbon Liquids, *Ground Water Monitoring and Remediation, 20*(3), 147-158, 2000.

Charbeneau, R.J., *Groundwater Hydraulics and Pollutant Transport*, Prentice Hall, Upper Saddle River, N.J., 2000.

Johns, R.T., L.W. Lake, A.B. Obigbesan, L. Bermudez, M.R. Hassan and Charbeneau, R.J., Analytical Solutions for Free-product Recovery using Skimmer and Dual-pump Wells, *Ground Water Monitoring and Remediation, 23*(1), 97-106, 2003.

Lenhard, R.J., Parker, J.C., and Mishra, S., On the Correspondence between Brooks-Corey and van Genuchten Models, *Journal of Irrigation and Drainage Engineering, 15*(4), 744-751, 1989.

Leverett, M.C., Capillary Behavior in Porous Media, *Trans. A.I.M.E. 142*, 341-358, 1941.

Mualem, Y., A New Model for Predicting the Hydraulic Conductivity of Unsaturated Porous Media, *Water Resources Research, 12*, 513-522, 1976.

van Genuchten, M.T., A Closed-form Equation for Predicting the Hydraulic Conductivity of Unsaturated Soil, *Soil Sci. Soc. Am. J., vol. 44*, 892-898, 1980.

APPENDIX A – HETEROGENEOUS SYSTEM

A.1 Introduction

In this appendix, the LNAPL free-product recovery models are extended for a simple case of aquifer heterogeneity where a soil layer of one texture overlies a layer with a differing texture, with an abrupt interface separating the layers. This case of soil heterogeneity is shown in Figure A.1. This figure shows a monitoring well with an LNAPL layer located between the air-NAPL interface z_{ao} and the NAPL-water interface z_{ow}. The total monitoring well thickness is b_o (not shown). The elevation of the water table, z_{aw}, provides the datum for fluid levels. While the water table is not present because of the LNAPL layer, its elevation is easily determined from the elevations z_{ao} and z_{ow}, and the LNAPL density ρ_o. For the example shown in Figure A.1, the abrupt facies interface between the upper Layer 1 and the lower Layer 2 is at elevation z_{12} located beneath the water table. This interface could be located above, below, or at the water table, and the texture characteristics of each layer and there contrast across the interface will strongly influence the resulting LNAPL saturation distribution. Figure A.1 should be compared with Figure 1.1.

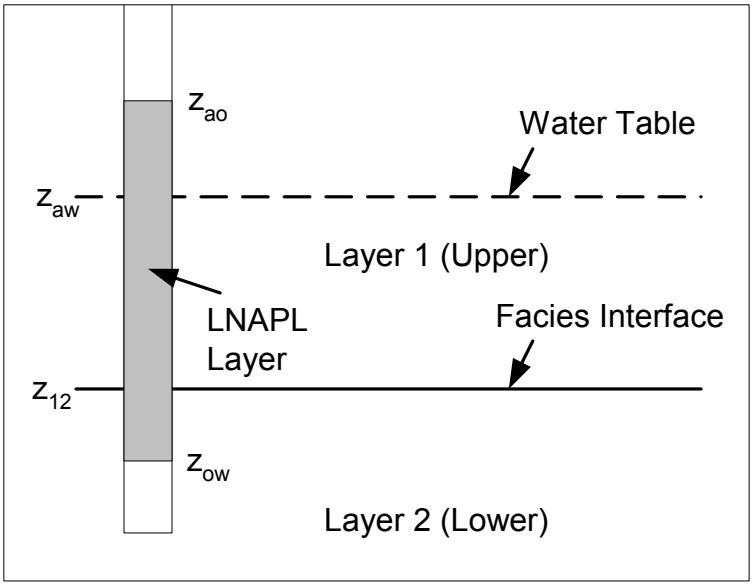

Figure A.1. Simple heterogeneity (abrupt facies interface) in subsurface porous media

For the heterogeneous soil system, the texture characteristics that must be defined for each layer include the porosity n, the van Genuchten parameters N and α, the irreducible water saturation S_{wr}, and the residual LNAPL saturation values for the vadose zone and saturated zone, S_{orv} and S_{ors}. Fluid properties include the LNAPL density ρ_o (it is assumed that the water density is 1 g/cm^3), and the water and LNAPL surface and interfacial tensions, σ_{aw}, σ_{ao}, and σ_{ow}.

A.2 Capillary Pressure Relationships

Equation 2.1 and appropriately scaled capillary pressure relationships are still used to describe the vertical distribution of fluid saturation, based on the assumption of vertical equilibrium. The pressure in each phase satisfies the hydrostatic pressure equation. Appreciation of this requirement is especially important when one considers porous media with abrupt changes in soil texture; the capillary pressure must remain continuous across an abrupt facies change, even though this results in an abrupt change in fluid saturation.

A.2.1 Saturation and Specific Volume for Heterogeneous Media

A simple case of aquifer heterogeneity is the condition where a soil layer of one texture overlies a layer with a differing texture, with an abrupt interface separating the layers. With the van Genuchten soil characteristic model, the parameters that must be specified include those for the upper layer, n_1, N_1, α_1, S_{wr1}, S_{orv1}, S_{ors1}, K_1, those for the lower layer, n_2, N_2 and a_2, S_{wr2}, S_{orv2}, S_{ors2}, K_2, and the elevation of the interface between the layers, z_{12}. Within this appendix and model description, layer 1 is the upper layer and layer 2 is the lower soil layer. Requirements from fluid mechanics dictate that under conditions of vertical equilibrium, the hydrostatic pressure remains continuous across the interface between the two layers, and that the fluid saturations adjust abruptly to local soil characteristic properties. This results in a discontinuity in fluid saturation values. Equations 2.13, 2.14 and 2.15 are applicable for both layers when appropriate layer-specific parameter values are used, and equation 2.24 may still

be used to calculate the specific free-product volume, D_o. The elevations z_{ow} and z_{ao} are independent of soil texture (see equations 2.19 and 2.20), while the elevation of z_{max} depends on local soil-texture properties.

As an example, Figure A.2 shows the water and LNAPL saturation distribution for conditions with an upper soil layer having properties $n_1 = 0.40$, $N_1 = 1.5$, $\alpha_1 = 0.5$ ft^{-1}, $S_{wr1} = 0.60$, $S_{orv1} = 0.05$, $S_{ors1} = 0.10$, and lower soil layer having properties $n_2 = 0.35$, $N_2 = 4.0$, $\alpha_2 = 2.0$ ft^{-1}, $S_{wr2} = 0.10$, $S_{orv2} = 0.10$, $S_{ors2} = 0.20$. The elevation of the interface between these layers is $z_{12} = -0.40$ feet. These properties correspond to the lower layer having a coarser soil texture than the upper layer, with an abrupt change in water saturation across the interface between the lower and upper layers. The LNAPL specific volume for the monitoring well thickness $b_o = 2$ feet is $D_o = 0.295$ feet. This compares with a specific volume $D_o = 0.499$ feet which is found if the soil profile is homogeneous with properties corresponding to the lower soil layer and $D_o = 0.158$ feet.

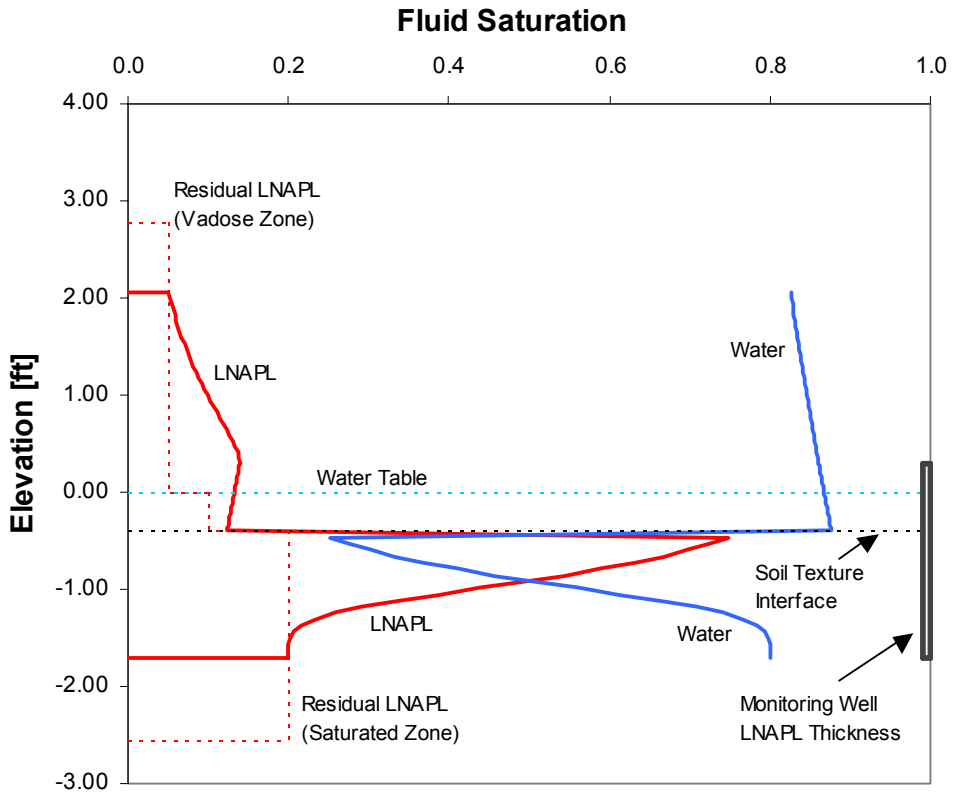

Figure A.2. LNAPL and water distributions for heterogeneous soil with properties corresponding to coarse texture layer overlying fine texture layer. Monitoring well LNAPL thickness equals 2 feet.

A.2.2 LNAPL-Layer Relative Permeability

The presence of soil heterogeneity can have a significant effect on the LNAPL-layer relative permeability function. Figure A.3 shows the relative permeability curve for the Mualem model for the conditions of Figure A.2 and for two homogeneous cases with coarse and fine-textured layers. The curve with triangle symbols corresponds to conditions shown in Figure A.2. The curve with diamond symbols is for a homogeneous soil with properties of the upper fine-grain soil in Figure A.2, while the curve with square symbols is for a homogeneous soil with properties of the lower coarse-texture soil. For small lens thickness, the lens is situated only in the fine-texture soil, and the relative permeability is the same as would be found for a homogenous fine-texture soil. Once the LNAPL-layer thickness exceeds about 1.2 feet, a significant part of the lens exits in the coarse-texture soil with larger saturation values and a higher effective LNAPL-layer relative permeability. Thus the curve rises above that of the homogeneous fine-texture soil.

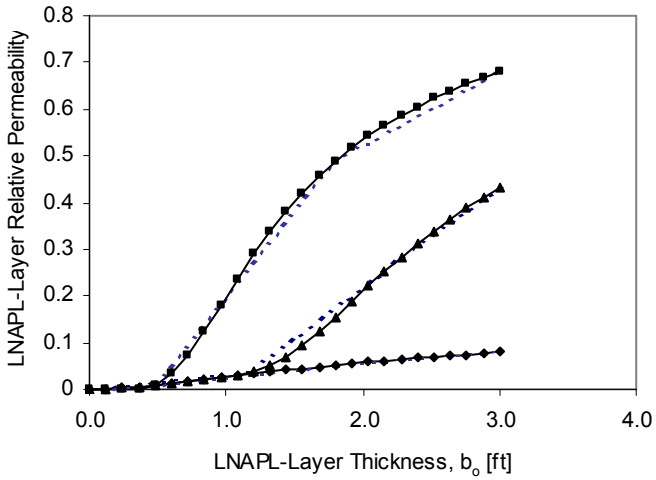

Figure A.3. LNAPL-layer relative permeability function for homogeneous coarse-texture soil (square), heterogeneous soil with fine-texture soil overlying coarse-texture soil (triangle), and homogeneous soil with fine-texture (diamond).

A.2.3 Spreadsheet Models for Heterogeneous Soil

The models described in Sections 3 and 4 have been also been implemented for heterogeneous soils through two separate and standalone spreadsheets: *LNAPL (vG-B-2L).xls and LNAPL (vG-M-2L).xls.* These are the two layer versions of the spreadsheet models described in Section 4, and the description remains basically the same except that additional soil texture data is required for the Data Entry sheet. For example, Figure A.4 shows the Data Entry worksheet used to develop Figure A.2.

van Genuchten-Mualem Model

Enter Data in Yellow Region

Maximum Monitoring Well LNAPL Thickness [feet]	
b_o =	3.000

Fluid Characteristics:		
ρ_o =	0.850	LNAPL density [gm/cc]
σ_{aw} =	65.000	air/water surface tension [dyne/cm]
σ_{ao} =	25.000	air/LNAPL surface tension [dyne/cm]
σ_{ow} =	15.000	LNAPL/water surface tension [dyne/cm]

Soil Characteristics:		
z_{12} =	-0.4	elevation of soil facies interface [ft]

Soil Layer 1 (Upper)		
n_1 =	0.400	porosity
N_1 =	1.500	van Genuchten "N"
α_1 =	0.500	van Genuchten "α" [ft^{-1}]
S_{wr1} =	0.600	irreducible water saturation
S_{orv1} =	0.050	residual LNAPL saturation (vadose)
S_{ors1} =	0.100	residual LNAPL saturation (saturated)

Soil Layer 2 (Lower)		
n_2 =	0.350	porosity
N_2 =	4.000	van Genuchten "N"
α_2 =	2.000	van Genuchten "α" [ft^{-1}]
S_{wr2} =	0.100	irreducible water saturation
S_{orv2} =	0.100	residual LNAPL saturation (vadose)
S_{ors2} =	0.200	residual LNAPL saturation (saturated)

Figure A.4. "Data Entry" worksheet showing data leading to Figure A.2

A.2.4 Model Implementation: Specific Retention and Hydraulic Contuctivity

There are two areas for which the model implementation must be modified to address the condition with heterogeneous soils with two layers having different soil texture properties. Because the LNAPL layer thickness changes through time during recovery operations, the LNAPL layer specific retention and effective hydraulic conductivity may also change. First consider the necessary modifications to address LNAPL volume and specific retention.

Equations 3.5, 3.6 and 3.7 must be modified for heterogeneous soil profiles. If $z_{ao} > z_{12} > 0$ [$b_o > z_{12}/(1-\rho_r)$] then equation 3.5 becomes

$$V_{or}(b_o) = \pi R_c^2 \left[n_1 S_{orv1}(z_{ao} - z_{12}) + n_2 S_{orv2} z_{12} - n_2 S_{ors2} z_{ow} \right]$$

This equation may be re-written as

$$V_{or}(b_o) = \pi R_c^2 \left\{ \left[(1-\rho_r) n_1 S_{orv1} + \rho_r n_2 S_{ors2} \right] b_o + (n_2 S_{orv2} - n_1 S_{orv1}) z_{12} \right\} \qquad (A.1)$$

If $z_{12} > z_{ao}$ [$b_o < z_{12}/(1-\rho_r)$] then equation 3.5 is appropriate with porosity and residual saturation values corresponding to layer 2. If $0 > z_{12} > z_{ow}$ [$b_o > -z_{12}/\rho_r$], then equation 3.5 takes the form

$$V_{or}(b_o) = \pi R_c^2 \left[n_1 S_{orv1} z_{ao} - n_1 S_{ors1} z_{12} + n_2 S_{ors2}(z_{12} - z_{ow}) \right]$$

Again, this equation may be re-written in the following form

$$V_{or}(b_o) = \pi R_c^2 \left\{ \left[(1-\rho_r) n_1 S_{orv1} + \rho_r n_2 S_{ors2} \right] b_o + (n_2 S_{ors2} - n_1 S_{ors1}) z_{12} \right\} \qquad (A.2)$$

If $z_{12} < z_{ow}$ [$b_o < -z_{12}/\rho_r$] then equation 3.5 is appropriate with porosity and residual saturation values corresponding to layer 1.

For the general case, when combined with equation 2.25, equation 3.6 may be written

$$V_o(b_o) = \pi R_c^2 (\beta - \gamma_{ij}) b_o + \delta \qquad (A.3)$$

where δ is a constant and

$$\gamma_{ij} = (1-\rho_r) n_i S_{orvi} + \rho_r n_j S_{orsj} \qquad (A.4)$$

The parameter γ_{ij} plays the same role in continuity for the LNAPL layer as the specific retention plays in continuity at the water table of an unconfined aquifer, as the water level rises and falls. In this regard, $(\beta - \gamma_{ij})$ plays the role of the specific yield (Charbeneau, 2000).

Most of the workbook calculations are straightforward and are based on the equations presented in Sections 2 and 3. However, calculations for both the skimmer well and trench require the medium hydraulic conductivity value, and for the two-facies heterogeneous model, its specification is problematic. Effects of two facies show up in two different parts of the calculations. Characteristics of soil texture that are represented by van Genuchten parameter values are implicitly included within the

functions $D_o(b_o)$ and $k_{ro}(b_o)$, and there fitted linear-segment models. However, the value of K_w also appears explicitly in both models.

One approach for dealing with variation in K_w with b_o would be to explicitly include it in calculation of the permeability distribution, so that one would calculate $K_o(b_o)$ rather than $k_{ro}(b_o)$. However, the additional contrast with including K_w variations in this function would make convergence of the approximating integrals to evaluate lens properties especially difficult (more so than the already included soil texture properties, as shown in Figure 4.4, for example). This approach has not been selected. Instead, variations in effective K_w values are included in the following 'ad hoc' fashion.

Effect of variation in K_w is directly related to the facies contact with the monitoring well LNAPL-thickness. This allows one to calculate an effective transmissivity, just as one would for a stratified aquifer with horizontal flow. If the facies discontinuity horizon lies within the range z_{ow}-z_{ao}, as shown in Figure A.1, then the effective hydraulic conductivity is calculated from

$$\overline{K}_w = \left(\left(z_{ao} - z_{12}\right)K_{w1} + \left(z_{12} - z_{ow}\right)K_{w2}\right)/b_o \qquad \text{(A.5)}$$

An added difficulty in calculation of free-product recovery rates is that $\overline{K}_w$ varies with LNAPL-layer thickness. Without explicitly including this effect, it is included in the recovery rate equations by using an effective hydraulic conductivity calculated from

$$\overline{\overline{K}}_w\left(b_{o1}, b_{o2}\right) = \sqrt{\overline{K}_w\left(b_{o1}\right)\overline{K}_w\left(b_{o2}\right)} \qquad \text{(A.6)}$$

Equation A.6 states that the effective hydraulic conductivity over a time period during which the LNAPL-layer thickness decreases from b_{o1} to b_{o2} is equal to the geometric mean value of the endpoint values.

APPENDIX B – VISUAL BASIC FUNCTION CALLS

```
Function bot(t, t3, t2, t1, bo1, bo2, bo3, b1, b2, b3, x2, x3, h1, h2, h3, _
             aw, aa, ask, ro, z12, por1, sorv1, sors1, por2, sorv2, sors2, _
             kw1, kw2)
    'Determine monitoring-well LNAPL thickness at time t
    '-------------------------------------------------
    '  t2 -> bo2  :  t1 -> bo1  :  t3 -> bz  :  x1 = 0


Function bo_trench(t, t3, t2, t1, bo1, bo2, bo3, b1, b2, b3, x2, x3, _
                   h1, h2, h3, ro, z12, por1, sorv1, sors1, por2, _
                   sorv2, sors2, kw1, kw2, dft, lt, jw, mo)
    'Determine monitoring-well LNAPL thickness at time t
    '-------------------------------------------------
    't2 -> bo2   :   t1 -> bo1   :   t3 -> bz   :   x1 = 0
    'dft = qt / (2 * wt * bt)       Darcy flux into trench


Function elev(index, bo, ro, z12, N1, aao1, aow1, swr1, sorv1, sors1, _
              N2, aao2, aow2, sw2, sorv2, sors2)
    'This function sorts out the elevation data for plotting saturation
    'and permeability profiles. The key elevations are zow, zao, zmax, and
    'z12. Depending on the magnitude of z12 compared with the others, there
    'may be two or three segments to the profile.


Function gg(bo, ro, z12, por1, sorv1, sors1, por2, sorv2, sors2)
    'Calculate the specific retention parameter "gamma"


Function hycon(bo, ro, z12, kw1, kw2)
    'Calculate the average water hydraulic conductivity corresponding
    'to LNAPL thickness bo, LNAPL density ration ro, and facies
    'interface elevation z12 in same units as kw1 and kw2


Function kro(z, bo, ro, z12, N1, aao1, aow1, swr1, N2, aao2, aow2, swr2)
    'Calculate the LNAPL relative permeability at elevation z using the
    'Burdine equation


Function krob(bo, ro, z12, N1, aao1, aow1, swr1, N2, aao2, aow2, _
              swr2, Eps_kro)
    'Evaluate the LNAPL-layer relative permeability


Function kro_b(bo, bo1, bo2, x2, x3, h1, h2, h3)
    'Determine LNAPL layer relative permeability based on bo using the
    'piecewise linear model and parameters from the "Layer Calcs" worksheet


Function qair(ha, lw, kra, kw1, kw2, rw, rc, z12)
    'Calculation of the well pressure due to vapor-enhanced recovery
```

```
Function sw(z, bo, ro, z12, N1, aow1, swr1, sors1, N2, aow2, swr2, sors2)
    'Calculate the water saturation at elevation z


Function so(z, bo, ro, z12, N1, aao1, aow1, swr1, sorv1, sors1, N2, aao2, _
            aow2, swr2, sorv2, sors2)
    'Calculate the LNAPL saturation at elevation z


Function swell(qw, bw, kw1, kw2, z12, ri, rw)
    'Calculate the drawdown at the well due to aquifer pumping


Function tmrec(index, t1, t2, t3, trec)
    'Order the sequence of times t1, t2, t3 and trecovery.
    'Return the time corresponding to "index", with 10
    'increments between each time epoch.


Function tt1(bo1, bo2, b2, x2, h2, aw, aa, ask, t2, ro, z12, por1, sorv1, _
             sors1, por2, sorv2, sors2, kw1, kw2)
    'Time to end of second segment of performance curve. Check whether
    'interface z12 is reached.


Function tt2(bo2, bo3, b3, x3, h3, aw, aa, ask, ro, z12, por1, sorv1, _
             sors1, por2, sorv2, sors2, kw1, kw2)
    'Time to end of first segment of performance curve. Check whether
    'interface z12 is reached.


Function tt3(bo1, bo2, bo3, b1, b2, b3, x2, x3, h1, h2, h3, aw, aa, ask, _
             ro, z12, por1, sorv1, sors1, por2, sorv2, sors2, kw1, kw2)
    'Return the time at which the LNAPL interface, determined by bo, reaches
    'the elevation of the facies-change interface z12


Function tt1_trench(bo1, bo2, b2, x2, h2, t2, ro, z12, por1, sorv1, sors1, _
             por2, sorv2, sors2, kw1, kw2, qt, lt, wt, bt, jw, mo)
    'Time to end of second segment of performance curve (bo2 -> bo1). Check
    'whether interface z12 is reached.


Function tt2_trench(bo2, bo3, b3, x3, h3, ro, z12, por1, sorv1, sors1, _
                    por2, sorv2, sors2, kw1, kw2, qt, lt, wt, bt, jw, mo)
    'Time to end of initial segment of performance curve (bo3 -> bo2). Check
    'whether interface z12 is reached.


Function tt3_trench(bo1, bo2, bo3, b1, b2, b3, x2, x3, h1, h2, h3, ro, z12, _
                    por1, sorv1, sors1, por2, sorv2, sors2, kw1, kw2, qt, _
                    lt, wt, bt, jw, mo)
    'Return the time at which the LNAPL interface, determined by bo, reaches
    'the elevation of the facies-change interface z12
```

```
Function vo(bo, ro, z12, por1, N1, aao1, aow1, swr1, sorv1, sors1, _
            por2, N2, aao2, aow2, swr2, sorv2, sors2, Eps_Do)
    'Evaluate the LNAPL specific volume corresponding to bo


Function vorecov(bo, bo1, bo2, bo3, b1, b2, b3, ro, z12, por1, sorv1, _
                 sors1, por2, sorv2, sors2)
    'Calculate the LNAPL recovery volume due to reducing the LNAPL
    'thickness from bo3 to bo

Function zmax(bo, ro, z12, N1, aao1, aow1, swr1, sorv1, sors1, N2, aao2, _
              aow2, swr2, sorv2, sors2)
    'Calculate the maximum elevation of free LNAPL
```

APPENDIX C – REPRESENTATIVE VAN GENUCHTEN MODEL PARAMETERS

(AFTER CARSELL AND PARISH, 1988)

Soil type	sample	Saturated Water Content, q_m		Residual Water Content, q_{wr}		van Genuchten N		van Genuchten a (ft^{-1})		Hydraulic Conductivity K_{ws} (ft/d)		
	size	mean	std. dev.	mean	std. dev.	mean	std. dev.	mean	std. dev.	sample size	mean	std. dev.
Clay	400	0.38	0.09	0.068	0.034	1.09	0.09	0.24	0.37	114	0.16	0.33
Clay Loam	364	0.41	0.09	0.095	0.010	1.31	0.09	0.58	0.46	345	0.20	0.56
Loam	735	0.43	0.10	0.078	0.013	1.56	0.11	1.1	0.64	735	0.82	1.44
Loamy Sand	315	0.41	0.09	0.057	0.015	2.28	0.27	3.8	1.3	315	11	8.9
Silt	82	0.46	0.11	0.034	0.010	1.37	0.05	0.49	0.21	88	0.20	0.26
Silt Loam	1093	0.45	0.08	0.067	0.015	1.41	0.12	0.61	0.37	1093	0.36	0.98
Silty Clay	374	0.36	0.07	0.070	0.023	1.09	0.06	0.15	0.15	126	0.016	0.085
Silty Clay Loam	641	0.43	0.07	0.089	0.009	1.23	0.06	0.30	0.18	592	0.056	0.15
Sand	246	0.43	0.06	0.045	0.010	2.68	0.29	4.4	0.88	246	23	12
Sandy Clay	46	0.38	0.05	0.100	0.013	1.23	0.10	0.82	0.52	46	0.095	0.22
Sandy Clay Loam	214	0.39	0.07	0.100	0.006	1.48	0.13	1.8	1.2	214	1.0	2.2
Sandy Loam	1183	0.41	0.09	0.065	0.017	1.89	0.17	2.3	1.1	1183	3.6	4.6

APPENDIX D – REPRESENTATIVE FLUID PROPERTIES

Interfacial and Surface Tension (dynes/cm) at 20° C

(From Charbeneau, et al. 1999. *Free-Product Recovery of Petroleum Hydrocarbon Liquids.* API Publication 4682)

Chemical Name	Interfacial Tension	Surface Tension
Benzene	35	28.9
Ethylbenzene	35.5	29.3
Toluene	36.1	28.5
o-Xylene	36.1	30.3
Crude Oil	no data	24-38
Diesel Fuel	50	25
Gasoline	50	21
Naptha (BTX mixture)	45	20
Fuel Oil No. 1	48	27
Jet Fuel JP-4/5	50	25
Petroleum Distillates	50	21

Source: Mercer, J.W. and Cohen, R. M., A Review of Immiscible Fluids in the Subsurface, *Journal of Contaminant Hydrology*, Vol. 6, pp. 107-163, 1990.

Laboratory measurements show that the values of both the surface and the interfacial tensions of a crude oil extend over a wide range of values, from 2 dyne/cm to 30 dyne/cm. A value of 25 dyne/cm is commonly used for both surface (σ_{ao}) and interfacial (σ_{ow}) tensions of a crude oil. Measurements show that for an unleaded gasoline with 7% MTBE, the interfacial tension is 35.1 dyne/cm (Charbeneau and Chiang, 1995). In the laboratory, the surface tension for water in contact with air is σ_{aw} = 72 dyne/cm. In soil, some chemicals will accumulate at the interface between water and air, reducing the surface tension, and an effective air-water surface tension of 65 dyne/cm is often assumed.

Additional information about interfacial tension values can be found in:

Kolhatkar R; Kremesec V, Rubin S, Yukawa C, Senn R. Application Of Field And Analytical Techniques To Evaluate Recoverability Of Subsurface Free Phase Hydrocarbons Proceedings Of The Petroleum Hydrocarbons And Organic Chemicals In Ground Water: Prevention, Detection, And Remediation; Conference And Exposition, November 17-19, 1999, Houston, Texas; p5-15.

LNAPL Parameters Database to be published by API in 2003. (Check www.api.org/lnapl for availability)

APPENDIX D – REPRESENTATIVE FLUID PROPERTIES (cont.)

Representative LNAPL Density Values (gm/cm^3)

(From Charbeneau, et al. 1999. *Free-Product Recovery of Petroleum Hydrocarbon Liquids.* API Publication 4682)

Fluid Type	Temp.0 °C	Source	Temp.15 °C	Source	Temp.20 °C	Source	Temp.25 °C	Source
Water	1.000	C	0.998	C	0.998	C	0.996	C
Automotive Gasoline	0.746	A	0.729	A				
Automotive Diesel	0.838	A	0.827	A				
Kerosene	0.842	A	0.839	A			0.835	A
Jet Fuel (JP-3)					0.800	B		
Jet Fuel (JP-5)			0.844	A	0.820	B		
Fuel Oil #2	0.874	A	0.866	A	0.840	A		
Fuel Oil #4	0.914	A	0.904	A	0.900	B	0.898	A
Fuel Oil #5	0.932	A	0.923	A			0.917	A
Fuel Oil #6 or Bunker C	0.986	A	0.974	A			0.964	A
Electrical Lubricating Oil	0.882	A	0.974	A				
Electrical Lubricating Oil – used	0.883	A	0.874	A				
Electrical Insulating Oil	0.892	A	0.882	A				
Electrical Insulating Oil – used	0.878	A	0.867	A				
Norman Wells Crude	0.845	A	0.832	A			0.829	A
Avalon Crude	0.846	A	0.839	A			0.834	A
Alberta Crude	0.850	A	0.840	A			0.832	A
Transmoutain Blend Crude	0.865	A	0.855	A				
Bow River Blend Crude	0.900	A	0.893	A			0.885	A
Prudhoe Bay Crude	0.915	A	0.905	A			0.900	A
Atkinson Crude	0.922	A	0.911	A			0.905	A
La Rosa Crude	0.923	A	0.914	A			0.908	A

Source: A-API, 1996; B-Mercer and Cohen, 1990; C-Vennard and Street, 1982

American Petroleum Institute, A Guide to the Assessment and Remediation of Underground Petroleum Releases, API Publication 1628, 3rd Ed., Washington, D.C., July 1996.

Mercer, J.W. and Cohen, R. M., A Review of Immiscible Fluids in the Subsurface, Journal of Contaminant Hydrology, Vol. 6, pp. 107-163, 1990.

Vennard, J. K. and R. L. Street, Elementary Fluid Mechanics (6th Edition), John Wiley and Sons, New York, NY, 1982.

APPENDIX E – REPRESENTATIVE POROSITY AND RESIDUAL SATURATION VALUES

Average Porosity (Standard Deviation) Values Based on Soil Texture

(From Charbeneau, et al. 1999. *Free-Product Recovery of Petroleum Hydrocarbon Liquids.* API Publication 4682)

Soil Type	Porosity (n)
Clay	0.38 (0.09)
Clay Loam	0.41 (0.09)
Loam	0.43 (0.10)
Loamy Sand	0.41 (0.09)
Silt	0.46 (0.11)
Silt Loam	0.45 (0.08)
Silty Clay	0.36 (0.07)
Silty Clay Loam	0.43 (0.07)
Sand	0.43 (0.06)
Sandy Clay	0.38 (0.05)
Sandy Clay Loam	0.39 (0.07)
Sandy Loam	0.41 (0.09)

(Source: Carsell, R. F. and Parish, R. S., Developing Joint Probability Distributions of Soil Water Retention Characteristics, *Water Resources Research*, 24(5), pp. 755-769, 1988.)

Descriptive Statistics from Carsel and Parrish (1988) Data Set Tabulated Values: Mean (Standard Deviation)

(From Charbeneau, et al. 1999. *Free-Product Recovery of Petroleum Hydrocarbon Liquids.* API Publication 4682)

Soil Type	Residual Saturation, S_{wr}	Bubbling Pressure Head, Ψ_b (m)*	Pore Size Distribution Index, λ
Clay	0.18 (0.089)	1.25 (1.88)	0.09 (0.09)
Clay loam	0.23 (0.024)	0.53 (0.42)	0.31 (0.09)
Loam	0.18 (0.030)	0.28 (0.16)	0.56 (0.11)
Loamy sand	0.14 (0.037)	0.081 (0.028)	1.28 (0.27)
Silt	0.074 (0.022)	0.62 (0.27)	0.37 (0.05)
Silty loam	0.15 (0.033)	0.50 (0.30)	0.41 (0.12)
Silty clay	0.19 (0.064)	2.0 (2.0)	0.09 (0.06)
Silty clay loam	0.21 (0.021)	1.0 (0.6)	0.23 (0.06)
Sand	0.10 (0.023)	0.069 (0.014)	1.68 (0.29)
Sandy clay	0.26 (0.034)	0.37 (0.23)	0.23 (0.19)
Sandy clay loam	0.26 (0.015)	0.17 (0.11)	0.48 (0.13)
Sandy loam	0.16 (0.041)	0.13 (0.066)	0.89 (0.17)

*Carsel and Parrish (1988) report mean and standard deviation of van Genuchten's 'a' parameter. The standard deviation of Ψ_b is approximated by:

$$\sigma_{\Psi_b} \cong \frac{\sigma_a}{\overline{a}^2}.$$

(Source: Carsell, R. F. and Parish, R. S., Developing Joint Probability Distributions of Soil Water Retention Characteristics, *Water Resources Research*, 24(5), pp. 755-769, 1988.)

APPENDIX E – REPRESENTATIVE POROSITY AND RESIDUAL SATURATION VALUES (cont.)

LNAPL Residual Saturation and Volumetric Retention Capacity Values (after Mercer and Cohen, 1990).

(From Charbeneau, et al. 1999. *Free-Product Recovery of Petroleum Hydrocarbon Liquids.* API Publication 4682)

Soil Type	R for Gasoline	Gasoline Residual Saturation	R for Middle Distillates	Middle Distillates Residual Saturation	R for Fuel Oil	Fuel Oil Residual Saturation
Coarse Gravel	2.5	0.007	5	0.014	10	0.029
Coarse Sand and Gravel	4	0.011	8	0.023	16	0.046
Medium to Coarse Sand	7.5	0.021	15	0.043	30	0.086
Fine to Medium Sand	12.5	0.036	25	0.071	50	0.143
Silt to Fine Sand	20	0.057	40	0.114	80	0.229
Coarse Sand		0.15 - 0.19				0.12
Medium Sand		0.12 - 0.27		0.19		0.11-0.23
Fine Sand		0.19 - 0.60				
Well Graded Sand		0.46 - 0.59				0.52

Residual LNAPL amounts are reported either in terms of residual saturation or *volumetric retention capacity,* R, defined by:

$$R = S_{or} \times n \times 1000$$

The units for R are liters of residual LNAPL per cubic meter of medium.

Source: Mercer, J.W. and Cohen, R. M., A Review of Immiscible Fluids in the Subsurface, *Journal of Contaminant Hydrology*, Vol. 6, pp. 107-163, 1990.

Additional information about residual saturation values can be found in:

> Brost, E.J., Devaull, G.E., *Non-Aqueous Phase Liquid (NAPL) Mobility Limits in Soil.* API Soil and Groundwater Research Bulletin No. 9 June 2000.

Additional copies are available through Global Engineering Documents at (800) 854-7179 or (303) 397-7956

Information about API Publications, Programs and Services is available on the World Wide Web at: http://www.api.org

American Petroleum Institute

1220 L Street, Northwest
Washington, D.C. 20005-4070
202-682-8000

Product No. I47290